Remote Sensing of Environment 115 (2011) 2360–2375

Contents lists available at ScienceDirect

Remote Sensing of Environment

journal homepage: www.elsevier.com/locate/rse

Assessing structural effects on PRI for stress detection in conifer forests

Rocío Hernández-Clemente [a,*], Rafael M. Navarro-Cerrillo [a], Lola Suárez [b], Fermín Morales [c], Pablo J. Zarco-Tejada [d]

[a] E.T.S.I.A.M.-Dpto. de Ingeniería Forestal, Universidad de Córdoba, Campus de Rabanales, 14071 Córdoba, Spain
[b] Remote Sensing Laboratories (RSL), Department of Geography, University of Zurich, Winterthurstr. 190, 8057 Zurich, Switzerland
[c] Estación Experimental Aula Dei (EEAD), Consejo Superior de Investigaciones Científicas (CSIC), Apdo. 13034, 50080 Zaragoza, Spain
[d] Instituto de Agricultura Sostenible (IAS), Consejo Superior de Investigaciones Científicas (CSIC), Alameda del Obispo, s/n, 14004 Córdoba, Spain

ARTICLE INFO

Article history:
Received 27 June 2010
Received in revised form 26 April 2011
Accepted 30 April 2011
Available online 28 May 2011

Keywords:
Forest decline
Water stress
Photosynthetic pigments
Airborne Hyperspectral Scanner
Photochemical-related indices

ABSTRACT

The retrieval of indicators of vegetation stress from remote sensing imagery is an important issue for the accurate assessment of forest decline. The *Photochemical Reflectance Index* (PRI) has been demonstrated as a physiological index sensitive to the epoxidation state of the xanthophyll cycle pigments and to photosynthetic efficiency, serving as a proxy for short-term changes in photosynthetic activity, stress condition, and pigment absorption, but highly affected by illumination conditions, viewing geometry and canopy structure. In this study, a diurnal airborne campaign was conducted over *Pinus sylvestris* and *Pinus nigra* forest areas with the *Airborne Hyperspectral Scanner* (AHS) to evaluate the effects of canopy structure on PRI when used as an indicator of stress in a conifer forest. The AHS airborne sensor was flown at two times (8:00 GMT and 12:00 GMT) over forest areas under varying field-measured stress levels, acquiring 2 m spatial resolution imagery in 80 spectral bands in the 0.43–12.5 μm spectral range. Five formulations of PRI (based on R_{531} as a xanthophyll-sensitive spectral band) were calculated using different reference wavelengths, such as PRI_{570} (reference band $R_{REF}=R_{570}$), and the PRI modifications PRI_{m1} ($R_{REF}=R_{512}$), PRI_{m2} ($R_{REF}=R_{600}$), PRI_{m3} ($R_{REF}=R_{670}$), and PRI_{m4} ($R_{REF}=R_{570}$, R_{670}), along with other structural indices such as NDVI, SR, OSAVI, MSAVI and MTVI2. In addition, thermal bands were used for the retrieval of the land surface temperature. A radiative transfer modeling method was conducted using the LIBERTY and INFORM models to assess the structural effects on the PRI formulations proposed, studying the sensitivity of PRI_m indices to detect stress levels while minimizing the effects caused by the conifer architecture. The PRI indices were related to stomatal conductance, xanthophyll epoxidation state (EPS) and crown temperature. The modeling analysis showed that the coefficient of variation (CV) for PRI was 50%, whereas the CV for PRIm1 (band R512 as a reference) was only 20%. Simulation and experimental results demonstrated that PRI_{m1} ($R_{REF}=R_{512}$) was less sensitive than PRI ($R_{REF}=R_{570}$) to changes in Leaf Area Index (LAI) and tree densities. PRI_{512} was demonstrated to be sensitive to EPS at both leaf ($r^2=0.59$) and canopy level ($r^2=0.40$), yielding superior performance than PRI_{570} ($r^2=0.21$) at the canopy level. In addition, PRI_{512} was significantly related to water stress indicators such as stomatal conductance (Gs; $r^2=0.45$) and water potential (Ψ; $r^2=0.48$), yielding better results than PRI_{570} (Gs, $r^2=0.21$; Ψ, $r^2=0.21$) due to the structural effects found on the PRI_{570} index at the canopy level.

1. Introduction

The Photochemical Reflectance Index (PRI) is a physiological reflectance index sensitive to the epoxidation state of the xanthophyll cycle pigments and to photosynthetic efficiency (Gamon et al., 1992). PRI was proposed by Gamon et al. (1992) as a normalized difference of 530 nm and a reference band at 550 nm, related to photosynthetic processes and affected by xanthophyll pigment absorption. Several studies report good results using 550 (or 551) nm as a reference wavelength (Middleton et al., 2009; Peñuelas et al., 1994). Based on research on leaves exposed to short-term changes in illumination, several studies (Gamon et al., 1993, 1997; Peñuelas et al., 1995) found that 570 nm appeared to be a better reference wavelength. Since then, PRI has been applied by using 570 nm as a standard reference at leaf and canopy levels (Sims & Gamon, 2002; Suárez et al., 2010). For example, the accumulation of de-epoxidated (DEPS) forms of xanthophyll cycle pigments was found by Peguero-Pina and co-workers in a silver fir stand growing under Mn deficiency (Peguero-Pina et al., 2007) and *Quercus coccifera* growing under intense drought (Peguero-Pina et al., 2008), assessing the stress effects on leaf PRI. Later, Filella et al. (2009) found significant correlation between PRI and DEPS across seasons and

* Corresponding author. Tel.: +34 957218657.
E-mail address: rociohc@uco.es (R. Hernández-Clemente).

0034-4257/$ – see front matter © 2011 Elsevier Inc. All rights reserved.
doi:10.1016/j.rse.2011.04.036

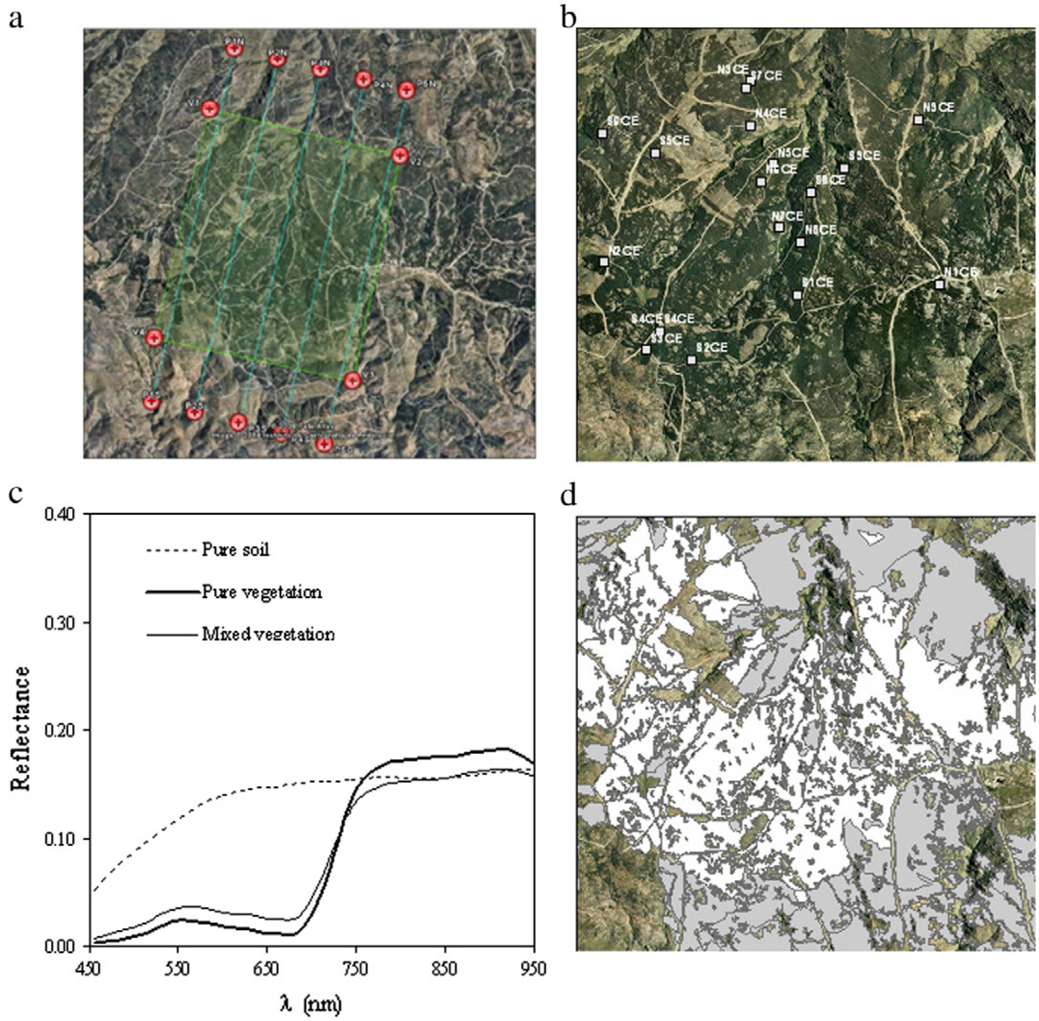

Fig. 1. AHS airborne footprint (a). Overview of the area acquired with the AHS instrument (b). Single pixel AHS spectra for pure vegetation, soil and mixed vegetation–soil pixels (c). Distribution of *Pinus sylvestris* (white) and *Pinus nigra* (gray) on the study area (d).

treatments for *Pinus sylvestris* and *Quercus ilex*. PRI was also related to carotenoid/chlorophyll ratio and b-carotene/chlorophyll ratio. It was only under brief variations in illumination conditions that PRI was correlated with DEPS, but was not related to other leaf pigments such as other carotenoids (Car) and chlorophyll a + b (Cab). Recent work (Suárez et al., 2009) demonstrated that PRI is a *pre-visual* water stress indicator in crops, but suggested that radiative transfer models were required to account for Cab and LAI effects for estimating the theoretical canopy PRI to help separating between stress levels. Nevertheless, such work relied on results obtained from tree crowns when targeting pure vegetation, thus causing smaller structural effects on PRI than forest canopy architectures. In addition, assessing plant physiological condition based on PRI at canopy scale is a difficult approach due to the different factors affecting this index, such as viewing and illumination geometry effects, crown architecture and shadow/sunlit fraction (Barton & North, 2001; Hall et al., 2008; Hilker et al., 2008; Middleton et al., 2009; Suárez et al., 2008).

Table 1
Structural parameters of *Pinus nigra* and *Pinus sylvestris* forest in the training areas. Mean values of age, height, basimetric area (BA) and min and max values of density.

Main species (Units)	Age (years)	Height (m)	Density (trees ha^{-1})	BA (m^2 ha^{-1})
Pinus sylvestris L.	35	7.99	1100–1895 (Mean: 1475)	26.55
Pinus nigra Arnold	40	8.60	950–2263 (Mean: 1594)	27.33

Table 2
Mean values and standard deviation of structural parameters calculated from the twelve trees measured in each study area for *Pinus sylvestris* (SS1, SS2, and SS3) *and Pinus nigra* (SN1, SN2, and SN3). Mean values of defoliation (%), basimetric area (BA), perimeter, height, stem height, trunk longitude, crown diameter and leaf area index (LAI).

Study area	BA (m^2 ha^{-1})	Perimeter (cm)	Height (m)	Stem height (m)	Trunk long. (m)	Crown diameter (m)	LAI
SS1	27.67 (±*3.78*)	49.61 (±*5.42*)	8.71 (±*0.93*)	2.16 (±*1.72*)	0.47 (±*0.02*)	3.13 (±*0.74*)	2.25 (±*0.02*)
SS2	22.00 (±*7*)	48.33 (±*4.47*)	7.97 (±*0.49*)	2.17 (±*0.147*)	0.64 (±*0.01*)	3.12 (±*0.41*)	2.36 (± *0.46*)
SS3	30.00 (±*4*)	41.72 (±*7.08*)	7.30 (±*0.55*)	1.76 (±*1.07*)	0.19 (±*0.42*)	2.82 (±*0.55*)	1.69 (±*0.19*)
SN1	32.33 (±*1.52*)	47.20 (±*8.76*)	8.95 (±*0.14*)	2.61 (±*0.00*)	1.71 (±*0.52*)	4.14 (±*0.68*)	1.90 (±*0.01*)
SN2	25 (±*4.35*)	38.98 (±*3.91*)	10.17 (±*1.25*)	3.98 (±*0.46*)	1.84 (±*0.00*)	3.23 (±*0.63*)	1.92 (±*0.19*)
SN3	24.66 (±*6.80*)	28.22 (±*2.71*)	6.70 (±*0.97*)	1.56 (±*1.27*)	0.55 (±*0.23*)	3.29 (±*0.45*)	2.28 (±*0.45*)

Table 3
Mean values and standard deviation of xanthophyll epoxidation state (EPS), water potential (Ψ) (Mpa) and stomatal conductance (Gs) (mmol H_2O m^{-2} s^{-1}) calculated for each study area for *Pinus sylvestris* and *Pinus nigra*. Measurements obtained at 12:00 GMT.

Study area	EPS	Ψ	Gs
Pinus sylvestris			
SS1 (Not stressed)	$0.85 \pm 0.08^{*}$	$-0.53 \pm 0.03^{*}$	$50.91 \pm 9.44^{*}$
SS2 (Moderate stress)	$0.75 \pm 0.11^{*}$	$-0.63 \pm 0.02^{*}$	$43.99 \pm 9.04^{*}$
SS3 (Stressed)	$0.58 \pm 0.14^{*}$	$-0.77 \pm 0.06^{*}$	$36.24 \pm 6.44^{*}$
Pinus nigra			
SN1 (Not stressed)	$0.85 \pm 0.05^{*}$	$-0.40 \pm 0.01^{*}$	$64.86 \pm 9.35^{*}$
SN2 (Moderate stress)	$0.80 \pm 0.11^{*}$	$-0.43 \pm 0.01^{*}$	$57.64 \pm 9.62^{*}$
SN3 (Stressed)	$0.70 \pm 0.10^{*}$	$-0.50 \pm 0.01^{*}$	$44.636 \pm 9.84^{*}$

* $p < 0.05$.

At the leaf level, additional PRI formulations have been proposed using varying reference wavelengths (Filella et al., 1996; Gamon et al., 1992; Inoue et al., 2008; Peñuelas et al., 1994). Many studies adopted 570 nm, largely based on the observation that it provided a good reference wavelength for leaf-level studies (Gamon et al., 1993, 1997; Peñuelas et al., 1995). At canopy scale, Gamon et al. (1992) showed how reflectance at several wavebands (from 539 to 670 nm) in combination with 531 nm worked rather well, and that 550 nm was the best overall reference wavelength based on a combination of statistical tests (regression, principle components analysis). This wavelength seemed to best correct for "greenness" (*i.e.*, canopy structure) effects. Other studies showed similar good results with 551 nm as a reference (the nearest MODIS band) (Middleton et al., 2009). Most authors adopted 570 nm as a reference, although the sensitivity of this index to structural and illumination effects were demonstrated (Suárez et al., 2008).

Forest decline is expressed through multiple effects due to an array of interacting biotic and abiotic factors. Assessing stress condition of a forest in decline using PRI is a complex problem because of the different alterations of the tree at the canopy- and stand-level (*e.g.*, changes in Leaf Area Index (LAI), Fraction of Photosynthetically Active Radiation (FPAR) and Leaf Angle Distribution (LAD), vegetation cover or stand density); at the leaf level, with alterations in photosynthetic activity, pigment content, and internal leaf structure; and at the cell level, with changes in water content, among others (Melzack et al., 1985). In the past, conifer forests in decline were assessed by changes in vegetation indices related to canopy structure, such as LAI (Schlerf et al., 2005; Schlerf & Atzberger, 2006), and chlorophyll concentration (Moorthy et al., 2008; Zarco-Tejada et al., 2004; Zhang et al., 2008). However, when canopy chlorophyll concentration or

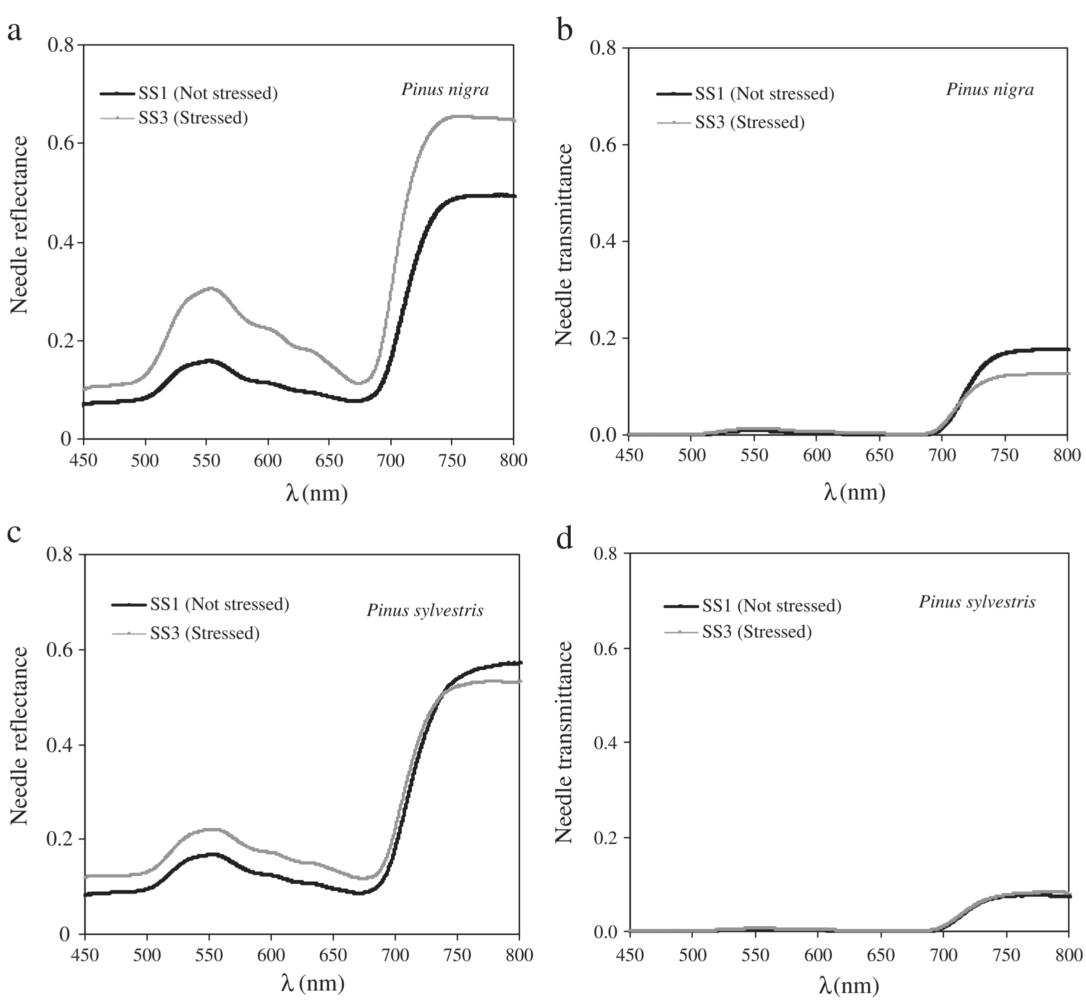

Fig. 2. Needle reflectance and transmittance measurements collected with a Li-Cor 1800–12 integrating sphere corresponding to *Pinus nigra* (a and b) and *Pinus sylvestris* (c and d) from stressed and non-stressed study areas.

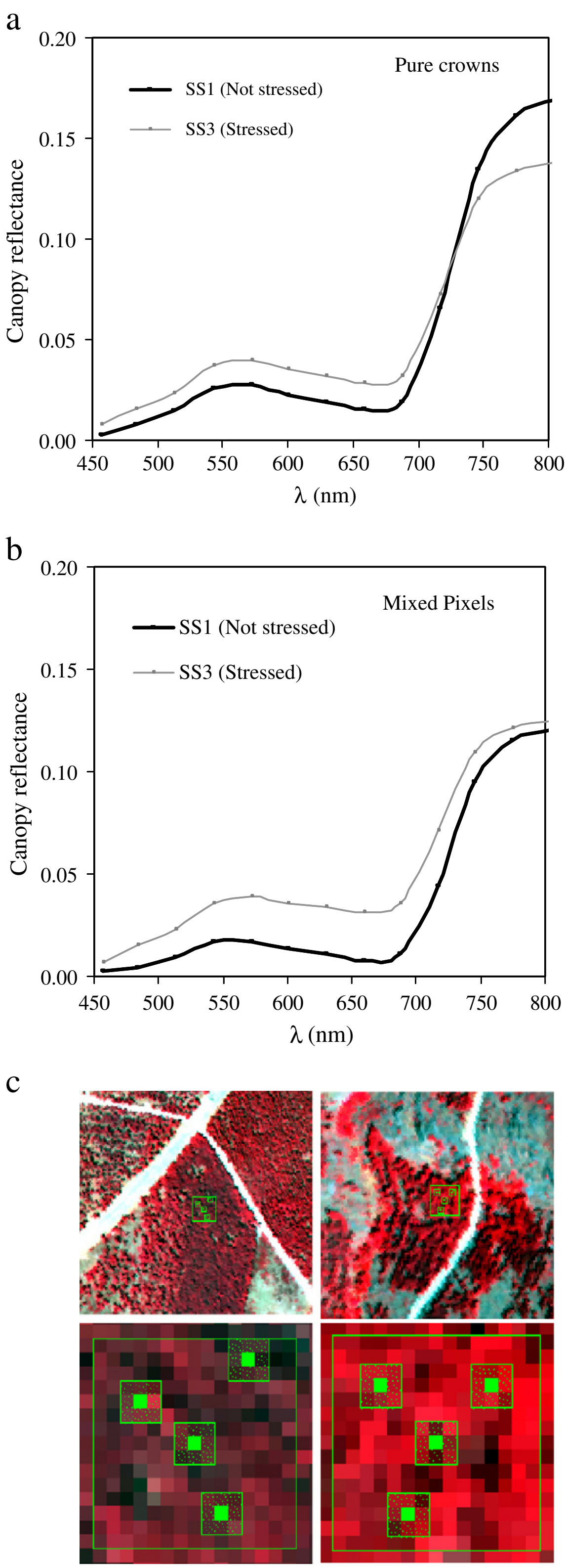

Fig. 3. AHS spectra for *Pinus sylvestris* of (a) pure tree crowns and (b) mixed pixels comprising pure crown, soil and shadow. (c) Example of stressed and non-stressed study areas for *Pinus sylvestris*.

Table 4
Photochemical reflectance index formulations and structural vegetation indices used in this study and indices calculated from the AHS bandset.

	Equation	Reference
PRI_{570}	$(R_{570}-R_{531})/(R_{570}+R_{531})$	Gamon et al. (1993)
PRI_{m1}	$(R_{512}-R_{531})/(R_{512}+R_{531})$	This study
PRI_{m2}	$(R_{600}-R_{531})/(R_{600}+R_{531})$	Gamon et al. (1993)
PRI_{m3}	$(R_{670}-R_{531})/(R_{670}+R_{531})$	Gamon et al. (1993)
PRI_{m4}	$(R_{570}-R_{531}-R_{670})/(R_{571}+R_{531}+R_{670})$	This study
NDVI	$(R_{NIR}-R_{red})/(R_{NIR}+R_{red})$	Rouse et al. (1974)
SR	(R_{NIR}/R_{red})	Jordan (1969); Rouse et al. (1974)
OSAVI	$(1+0.16)\ (R_{800}-R_{670})/(R_{800}+R_{670}+0.16)$	Rondeaux et al. (1996)
MSAVI	$\frac{1}{2}\left[2\,R_{800}+1-\sqrt{(2\,R_{800}+1)^2-8\,(R_{800}-R_{670})}\right]$	Qi et al. (1994)
$MTVI_2$	$\frac{1.5\,[1.2\,(R_{800}-R_{550})-2.5\,(R_{670}-R_{550})]}{\sqrt{(2\,R_{800}+1)^2-(6*R_{800}-5\,\sqrt{R_{670}})-0.5}}$	Haboudane et al. (2004)

total leaf area is affected by water stress, damage to the plant has already occurred, and plant status is compromised. The detection of stress in its early phase is normally defined as pre-visual and takes place before there are structural (visual) effects or consequences of the stress; this is critical information required for the assessment of forest decline. These processes related to water stress have affected important areas in Spain and other European countries (Allen et al., 2009; Martínez-Vilalta et al., 2008; Navarro-Cerrillo et al., 2007; Rebetez & Dobbertin, 2004). Such studies

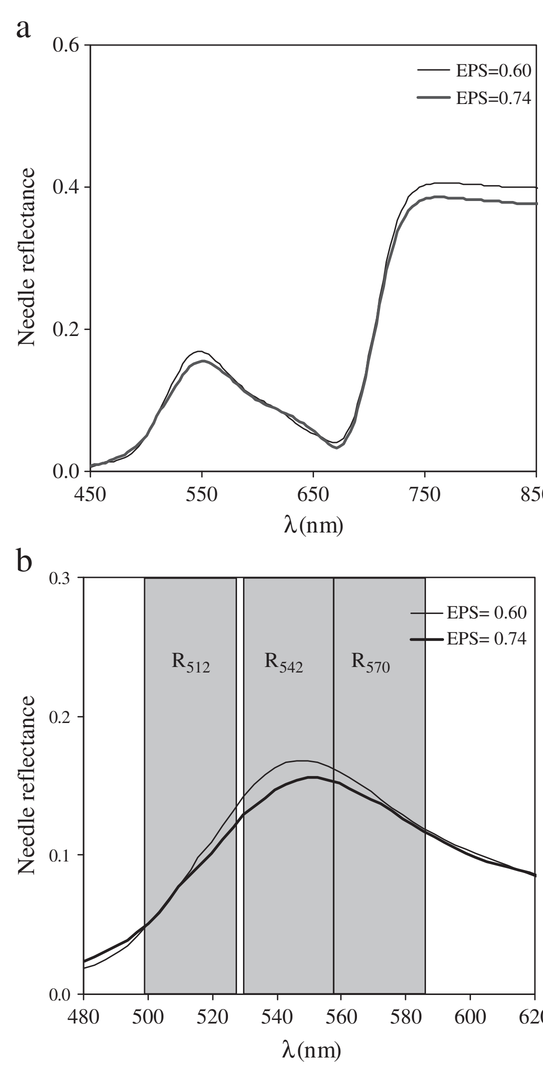

Fig. 4. (a) Spectral reflectance of needles of *Pinus sylvestris* with different epoxidation state of the xanthophylls (EPS) values. (b) Zoom of the region of absorption of the xanthophylls cycle and center wavelength and bandwidth for the AHS bands used to calculate PRI (R_{512}, R_{542}, and R_{571}). Measurements obtained at 12:00 GMT.

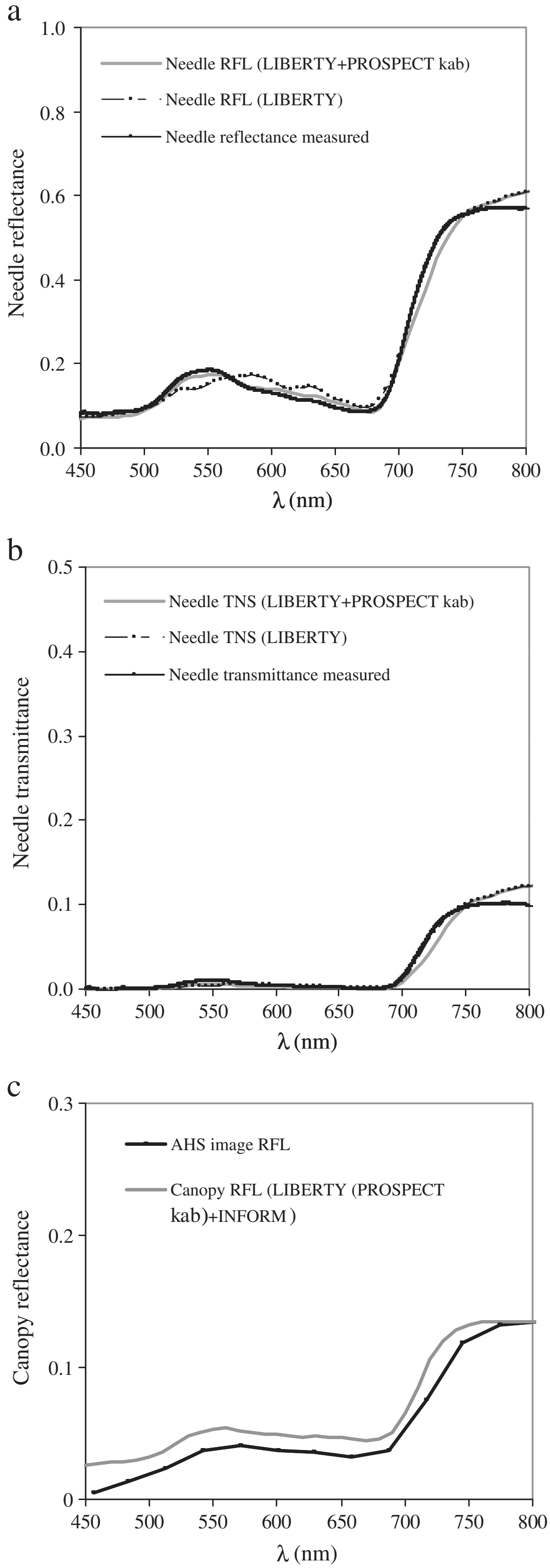

Fig. 5. Needle reflectance (RFL) (a) and transmittance (TNS) (b) measured with the integrating sphere, simulated with LIBERTY and simulated with LIBERTY using the absorption coefficient of PROSPECT. Crown reflectance spectra obtained from the AHS image and simulated with LIBERTY + INFORM (c).

Table 5
Nominal values and range of parameters used for leaf and canopy modeling with LIBERTY and INFORM for *Pinus nigra*.

	Units	Values
Leaf optical and structural parameters		
Hemispherical reflectance and transmittance of green leaves	nm	Measured
Average internal cell diameter (D)	µm	65
Intercellular air space determinant (*xu*)	/	0.06
Needle thickness	/	4.09
Linear (baseline) absorption	/	0.0006
Albino leaf absorption	/	1.25
Leaf Chl a + b content	mg/m^2	100–500
Leaf equivalent water	g/m^2	100
Lignin/cellulose content	g/m^2	40
Protein content	g/m^2	1
Canopy structural parameters		
LAI	m^2/m^2	1–3
No. trees/ha	/	800–2800
Crown height	m	7.9
Crown diameter	m	3.7
Background and viewing geometry		
Solar zenith and azimuth	Degrees	190.68
Instrument solar zenith and azimuth	Degrees	17.7
Soil reflectance	mm	Measured

demonstrate that drought plays an important role in Mediterranean forest decline, especially in species sensitive to water stress like *P. sylvestris* (Martínez-Vilalta et al., 2008; Poyatos et al., 2008). Research has shown that in an early stage of stress, before damage has occurred, photosynthesis declines. Under these conditions, the absorbed light exceeds the photosynthetic demand, and plants react with mechanisms for dissipating this excess energy non-destructively (Björkman & Demmig-Adams, 1994). One mechanism is linked to xanthophyll cycle activation, where pigment violaxanthin is converted into antheraxanthin and zeaxanthin via de-epoxidase reactions (Yamamoto, 1979). Several manuscripts have revealed a close correlationship between xanthophyll pigment conversions and excess energy dissipation in the leaf pigments associated with photosystem II (PSII) (Demmig-Adams & Adams, 1996). Another stress indicator suggested in several studies (proposed by Jackson et al., 1977) is the temperature of the canopy as an indicator of tree transpiration. Thermal remote sensing of water stress has been successfully applied to tree crop canopies based on high resolution thermal remote sensing imagery (Berni et al., 2009), airborne thermal imagery (Sepulcre-Cantó et al., 2007) and satellite thermal information in combination with 3D radiative transfer models to understand the effects of scene thermal components on large ASTER pixels (Sepulcre-Cantó et al., 2009).

However, very few references have shown feasible remote sensing methods for successfully linking remote sensing indices and physiological variables by focusing on the *pre-visual* detection of forest decline before damage is visible. At canopy scale, most of this research has dealt primarily with photosynthetic light use efficiency and carbon dioxide using satellite images such as the Moderate Resolution Imaging Spectroradiometer data (MODIS) (Drolet et al., 2005; Garbulsky et al., 2008; Hilker et al., 2009) or EO-1 Hyperion data (Asner et al., 2005). Nevertheless, few of these studies are focused on PRI and other spectral indices validated with *in situ* measurements of EPS in heterogeneous forest ecosystems. Questions need to be answered regarding PRI interpretation on forest canopies where crown mixture, shadows and tree architecture play a critical role in physiological remote sensing indices. The present study provides new insights into the understanding of PRI as an indicator of stress on complex canopies, analyzing the effects on PRI formulations due to the structure. The study assesses imaged PRI and model-simulated PRI

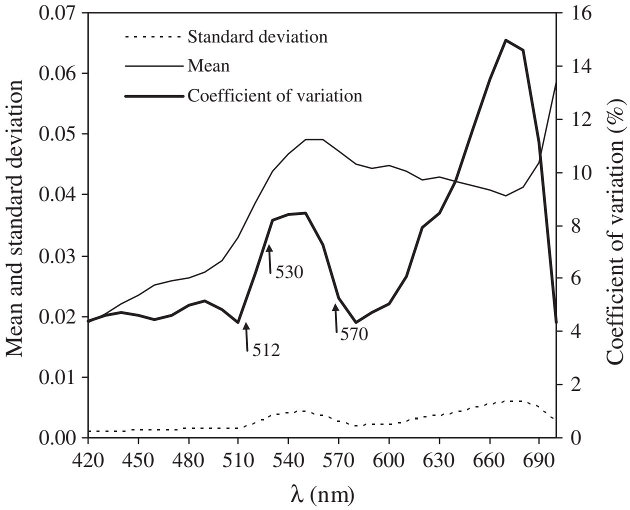

Fig. 6. Mean, coefficient of variation (CV), and standard deviation of spectral reflectance for LAI ranges (1–3) and tree densities (800–2800 trees/ha) simulated with the coupled LIBERTY + INFORM model.

obtained through radiative transfer simulation of conifer canopies, evaluating the sensitivity of PRI formulations to EPS while minimizing canopy structural effects.

2. Material and methods

2.1. Study area selection

The experimental area is located in Sierra de Filabres (Almeria province, southeastern Spain) (37° 13′ 27″ N, 2° 32′ 54″ W) (Fig. 1), the driest region in Western Europe. The elevation of the study area ranges from 1540 to 2000 m.a.s.l., and annual rainfall is between 300 and 400 mm. The annual average temperature is 11 °C, reaching a maximum of 32 °C during summer and a minimum of −8 °C during winter. The vegetation consists of a 40-year-old mixed pine afforestation of *Pinus nigra* Arnold and *P. sylvestris* L. (Tables 1 and 2). Within the forest stands, sparse evergreen shrub vegetation (*Adenocarpus decorticans* Boiss. and *Cistus laurifolius* L.) partially covers the ground. Parent material is composed of siliceous rock with quartz micaschists, forming eutric cambisol–regosol soils.

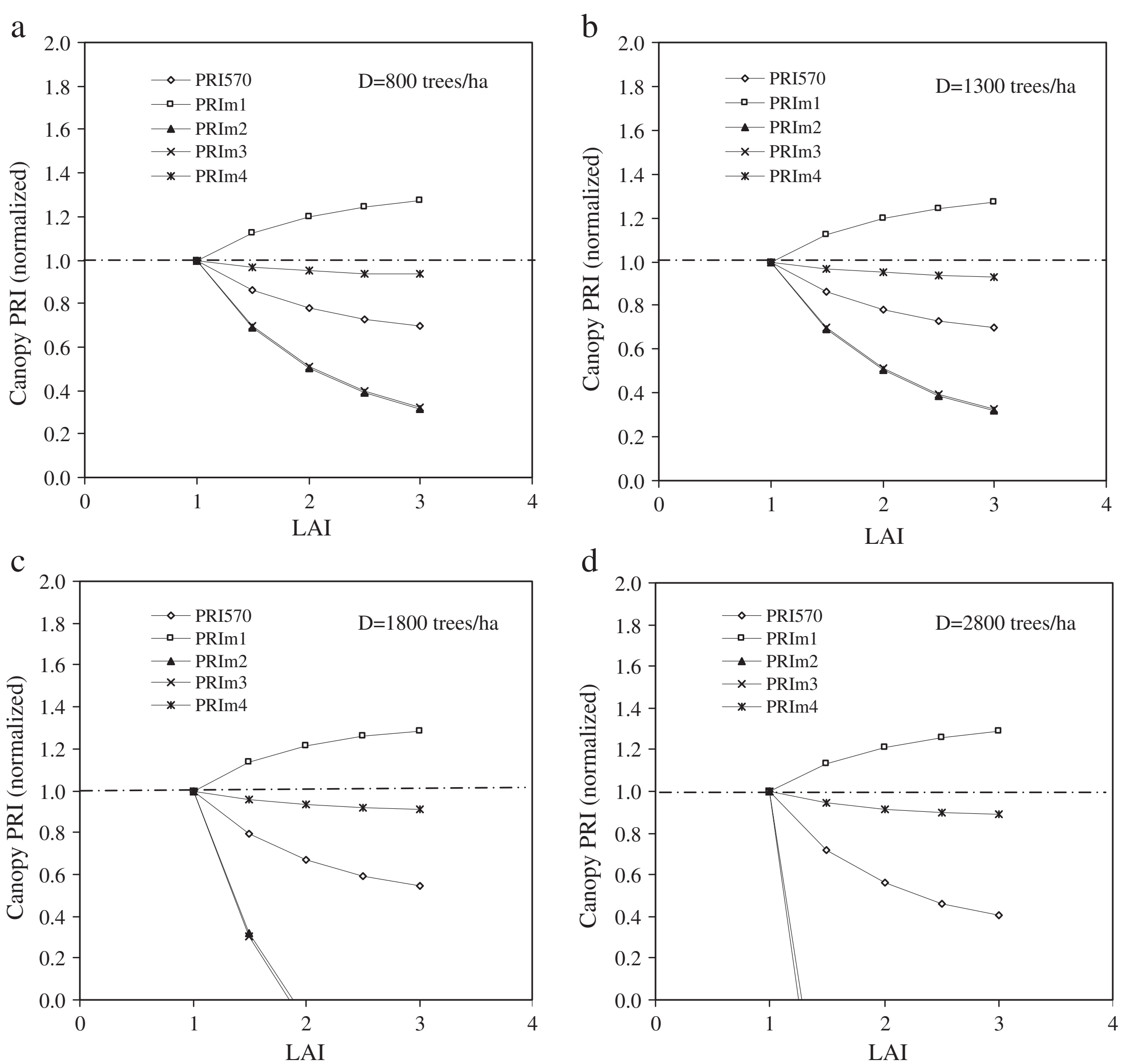

Fig. 7. Model simulations conducted with INFORM for PRI_{570} and modified PRI formulations. Results obtained by simulating the plot reflectance with different densities (D) and LAI values. Results normalized for LAI = 1. Tree densities (D) used were a) 800, b) 1300, c) 1800, d) 2800 trees/ha.

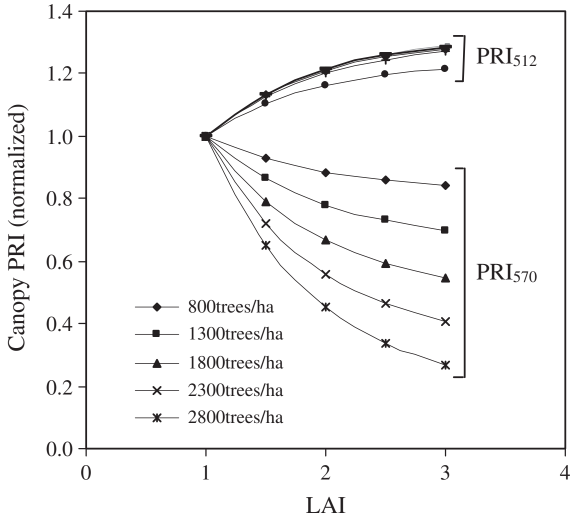

Fig. 8. Model simulations conducted with INFORM for PRI_{570} and PRI_{512}. Results obtained by simulating the plot reflectance with different densities (D) and LAI values. Results normalized to LAI = 1.

2.2. Field data collection

Field sampling campaigns were conducted concurrently with airborne overflights during the last week of July 2008. Two sets of measurements were collected at 8:00 and 12:00 (GMT). The monitored trees consisted of 36 *P. nigra* and 36 *P. sylvestris,* located in three study areas (12 trees per study areas). Table 3 shows the mean values and the standard deviation of xanthophyll epoxidation state (EPS), water potential (ψ) and stomatal conductance (Gs) calculated for each study area at 12:00 GMT. To test the null hypothesis that EPS, water potential, and stomatal conductance were not significantly different among study areas, a one-way ANOVA analysis was conducted using a significance level of 0.05. A Tukey's post-hoc analysis was performed to evaluate differences between study areas. In the case of water potential a Kruskal–Wallis (KW) test was applied because the data were not normally distributed. The variables measured showed significant differences in the physiological status for each study area ($p<0.05$).

The measurements were conducted on trees of similar height (Table 2) located in low slope areas (<10%), therefore with a similar sun/shade fraction. The trees are largely the same age since they were part of a reforestation program undertaken by the Spanish government in 1980.

Physiological parameters measured from the selected trees were total concentration of chlorophyll (chlorophyll a (chl_a) and chlorophyll b (chl_b)), needle water content and dry mass, stomatal conductance (using a portable gas exchange system CIRAS-1 instrument, PP Systems, Hitchin Herts, UK) and crown temperature (using an infrared thermometer, Optris LS, DE). These data were averaged from four measurements per tree during each period at the time of the AHS imagery acquisition (8:00 and 12:00, GMT). Field Gas exchange measurements were performed in attached leaves at controlled CO_2 external concentration (Ca = 350 ppm) and ambient relative humidity. Stomatal conductance (Gs) was estimated using gas exchange data and the total needle area exposed obtained from photos taken for each measurement. Predawn ($\Psi_{pd,}$ 4:00 GTM) and midday (Ψ_m, 12:00 GTM) xylem water potential (pressure chamber, SKPM 1400, Skye Instruments, UK) (Scholander et al., 1965) were also measured. LAI was estimated with a PCA (Plant Canopy Analyzer, LAI-2000, LI-COR, Lincoln, NE, USA).

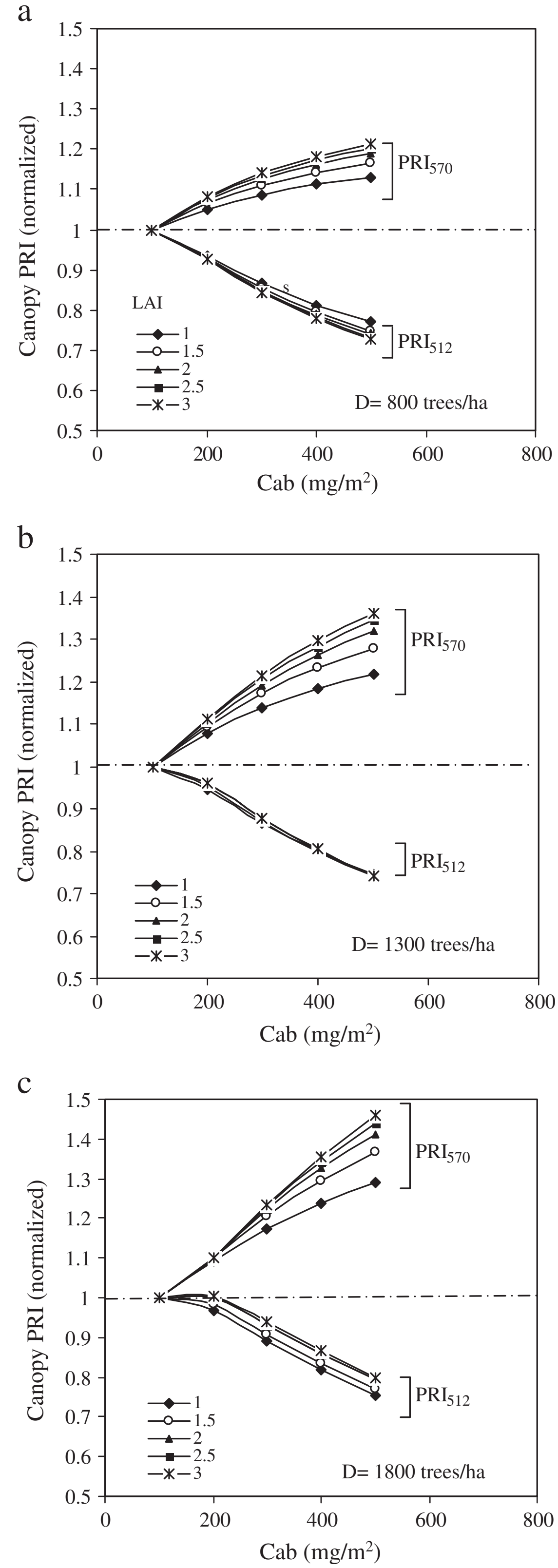

Fig. 9. Model simulations conducted with INFORM for canopy PRI_{570} and PRI_{512} for different values of chlorophyll (Cab). Results obtained by simulating the plot reflectance with different values of LAI for a) 800 trees/ha, b) 1300 trees/ha, c) 1800 trees/ha.

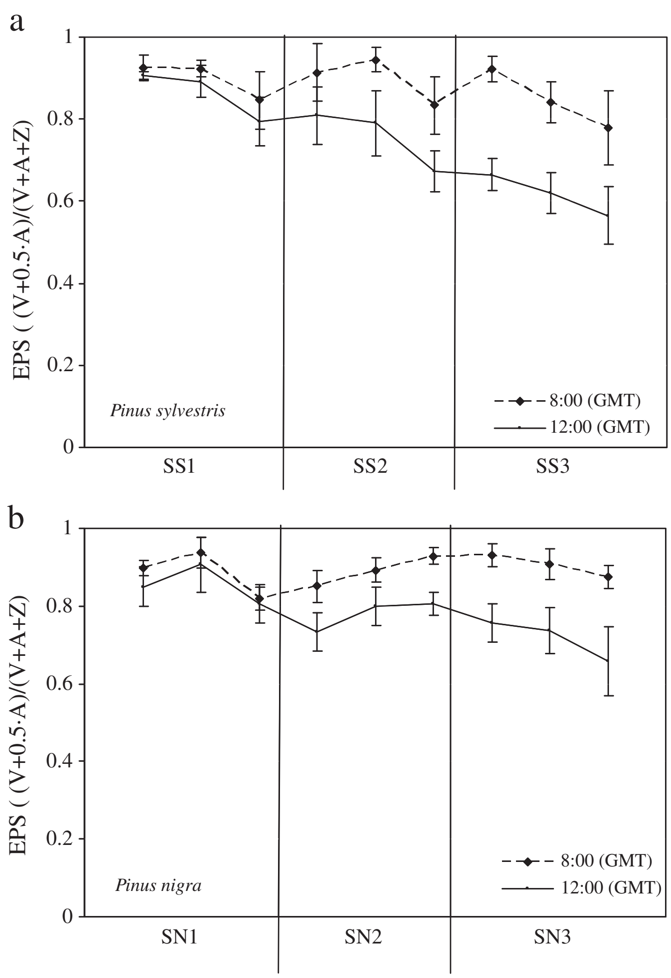

Fig. 10. Comparison between the epoxidation state of the xanthophylls pigments at 8:00 and 12:00 GMT measured at each study areas (SS1, SS2, and SS3) for *Pinus sylvestris* (a) and (SN1, SN2, and SN3) for *Pinus nigra* (b). The value on each plot is the mean EPS of the four trees measured per plot and the corresponding standard deviation.

2.3. Leaf-level measurements

Leaf-level measurements were collected on a total of 15 needles per tree, five needles per needle age (current-year, n; young, n + 1; and mature, n + 3), with a total of 540 needles measured per species. The needles were collected from the top of the crown by selecting branches of illuminated areas. Two sets of needles were collected from the same shoots at the time of the AHS flights, 8:00 and 12:00 (GMT). One set was placed under cold storage in coolers, and the other set was frozen in liquid nitrogen in the field. Both storage conditions were in darkness, and the needles were harvested and immediately frozen in the field. The first set was transported directly to the laboratory and used to measure leaf spectral reflectance and transmittance, and water content. The second set was kept under -80 °C and used for pigment analysis by destructive methods.

Needle pigments were extracted as reported by Abadía and Abadía (1993). Pigment extracts were obtained from a mixed sample of 5 cm of needle material, 1 linear cm per needle. The area was calculated by assuming the needle to be a half cylinder and the diameter to be the measured width of each needle. Needle diameter was measured with a digital caliper precision instrument. Pigment content was obtained based on this area. Five consecutive centimeters were also cut for structural measurements (thickness and width), water content and dry mass. The needles were ground in a mortar on ice with liquid nitrogen and diluted in acetone up to 5 ml (in the presence of Na ascorbate). Then, the extracts were filtered through a 0.45-µm filter to separate the pigment extracts from the Na ascorbate. The spectrophotometric and High-Performance Liquid Chromatography (HPLC) determinations were carried out simultaneously on the same extracts, 20 µl were injected into the HPLC and 1 ml was inserted into the spectrophotometer. The extractions and measurements were undertaken concurrently to avoid pigment degradation. Absorption at 470, 644.8 and 661.6 nm was measured with the spectrophotometer to derive chlorophyll *a* and *b*, and total carotenoid concentrations (Abadía & Abadía, 1993) and pigment extracts were analyzed using an isocratic HPLC method (Larbi et al., 2004). Samples were injected into a 100 × 8 mm Waters Novapak C18 radial compression column (4 µm particle size) with a 20 µl loop, and mobile phases were pumped by a Waters M45 high pressure pump at a flow of 1.7 ml/min. The EPS ratio between the pigment concentration was calculated as $(V+0.5A)/(V+A+Z)$ (Thayer & Björkman, 1990), where V is violaxanthin, A is antheraxanthin and Z is zeaxanthin.

Optical measurements were taken on needles from a total of 42 trees, 21 trees per species. Needle reflectance and transmittance were measured with a Li-Cor 1800–12 integrating sphere (Li-Cor, Lincoln, NE, USA) coupled to a fiber optic spectrometer (Ocean Optics model USB2000 spectrometer, Ocean Optics, Dunedin, FL, USA), using the method described in Moorthy et al. (2008) and Zarco-Tejada et al. (2004). Needle reflectance and transmittance measurements of *P. nigra* (Fig. 2a and b) and *P. sylvestris* (Fig. 2c and d) showed variations in the visible spectral region due to stress levels affecting both chlorophyll and xanthophyll pigments. Needle spectral reflectance was also measured with a UniSpec Spectral Analysis System (PP Systems, Herts, UK), following a similar procedure to that described by Richardson and Berlyn (2002). The Unispec measurements were conducted in the field minutes before the needles were collected.

2.4. Airborne image acquisitions

The airborne campaign was conducted by the Spanish Aerospace Institute (INTA) with the Airborne Hyperspectral Scanner AHS (Sensytech Inc., currently Argon St. Inc., Ann Arbor, MI, USA) during the last week of July 2008. The airborne data acquisition was carried out at 8:00 GMT and 12:00 GMT, acquiring 2 m spatial resolution imagery in 38 bands in the 0.43–12.5 µm spectral range. The Field of View (FOV) and Instantaneous Field of View (IFOV) of the AHS sensor were 90º and 2.5 mrad respectively, and plots were located in the central region of the scene in order to avoid edge effects. *At-sensor* radiance processing and atmospheric correction were performed at the INTA facilities. Atmospheric correction was conducted with ATCOR4 based on the MODTRAN radiative transfer model (Berk et al., 1998, 2000) using aerosol optical depth at 550 nm collected with a Micro-Tops II sun photometer (Solar Light, Philadelphia, PA, USA). Land surface temperature retrieval from thermal remote sensing data was obtained with the two-channel algorithm proposed by Sobrino et al. (2002, 2006), taking into account emissivity and water vapor effects. The emissivity value applied for vegetation was 0.98. A full description of land surface temperature retrieval from thermal imagery via AHS can be found in Sepulcre-Cantó et al. (2006) and Sobrino et al. (2006) . The mean air temperature during the flight was 20.9 °C (±0.05) at 8:00 GMT and 24.5 °C (±0.11) at 12:00 GMT. The temperature data were collected by the meteorological station at Calar Alto Astronomical Observatory, located within the study area.

Vegetation indices were calculated to track changes in canopy structure and pigment concentration as a function of the stress condition. The AHS spectra (Fig. 1c) were extracted from the imagery at windows of 3 × 3 pixels. Pure vegetation pixels were located by selecting the pixels with NDVI higher than 0.6 on 3 × 3 windows. Fig. 3 shows one region of interest extracted for affected and non-affected

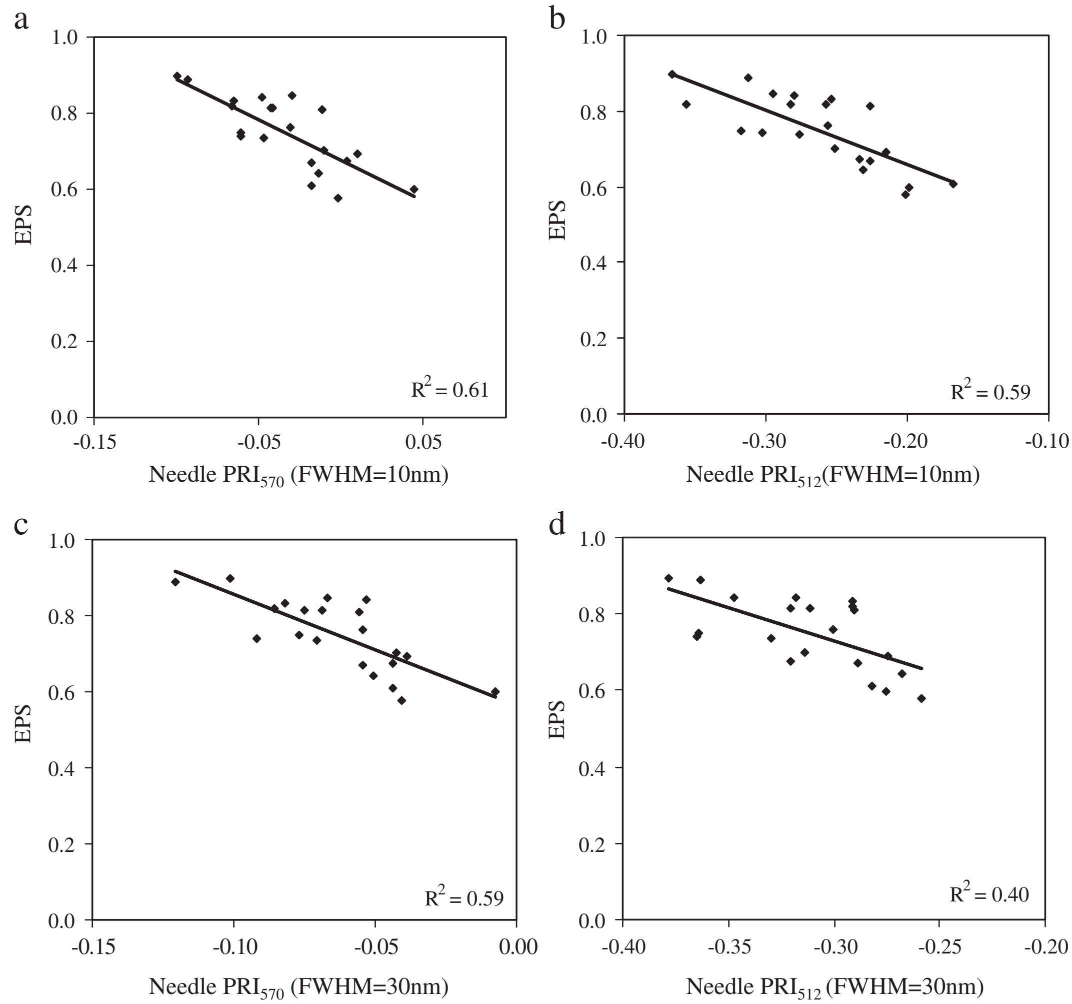

Fig. 11. Relationships obtained between the epoxidation state of the xanthophylls pigments EPS = (V + 0.5 A) / (V + A + Z) and PRI_{570} for FWHM of 10 nm (a) and 30 nm (c), and PRI_{512} with FWHM of 10 nm (b) and 30 nm (d). Needle measurements obtained at 12:00 GMT from crowns with different levels of stress on *Pinus sylvestris*.

areas of *P. nigra* and *P. sylvestris*. The airborne reflectance extracted for each tree, and comparing the spectra for stressed and non-stressed study areas (SS1 and SS3) of pure crowns and mixed pixels are shown in Fig. 3a and b, respectively.

Spectra extracted from the imagery were related to the field data using pure vegetation pixels (NDVI higher than 0.6). The analysis aimed at assessing the relationships between EPS, G and Ψ and the different PRI formulations calculated to minimize the structural effects on PRI. The index PRI was reformulated as derived from R_{531} (adapted to AHS using band R_{540} as in Suárez et al., 2008) using reference bands R_{512} (PRI_{m1}), R_{600} (PRI_{m2}), R_{670} (PRI_{m3}), and R_{670} and R_{570} (PRI_{m4}) (Table 4). The PRI formulations proposed in this study (Table 4) were based on the results obtained in previous work (Gamon et al., 1993; Jordan, 1969; Rouse et al., 1974) and on the spectral trend of the reflectance at the 500–600 nm region. Fig. 4a shows the needle spectral reflectance of *P. sylvestris* measured with a Unispec spectroradiometer for two stress levels at 12:00 GMT. As shown in Fig. 4b both regions at 500–520 nm and 570–590 nm could be used as a reference band. Fig. 4b also shows the bandwidth corresponding to AHS airborne sensor used to calculate PRI_{570} and PRI_{512}.

The indices were also normalized by structure-sensitive effects using indices such as NDVI (Rouse et al., 1974), SR (Jordan, 1969; Rouse et al., 1974), MTVI2 (Haboudane et al., 2004), OSAVI (Rondeaux et al., 1996) and MSAVI (Haboudane et al., 2004). Indices were adapted to the AHS bandset using the closest bands available.

2.5. Model simulation with LIBERTY and INFORM

Radiative transfer modeling methods were applied with the *Leaf Incorporating Biochemistry Exhibiting Reflectance and Transmittance Yields* (LIBERTY) model (Dawson et al., 1998) linked to the *Invertible Forest Reflectance Model* (INFORM) (Atzberger, 2000). LIBERTY was designed to model conifer (particularly pine) needles at the cellular scale, based on Melamed's radiative transfer theory of powders (Melamed, 1963). This model calculates reflectance and transmittance by assuming the needle structure to be cell spheres separated by air gaps. The LIBERTY and PROSPECT models were assessed by Zarco-Tejada et al. (2004) and Moorthy et al. (2008) suggesting that PROSPECT could be used to model needle optical properties. PROSPECT is a radiative model initially designed for broad leaves, although it was later adapted to needles (Malenovsky et al., 2006). In a recent paper, Di Vittorio (2009) enhanced the limitation of LIBERTY to resolve individual pigments and the gaps in the estimation of *in vivo* specific absorption coefficients and model biophysics. At canopy level, INFORM simulates the *bi-directional* reflectance of forest stands between 400 and 2500 nm, being a combination of the *Forest Light Interaction Model* (FLIM) (Rosema et al., 1992) and *Scattering by*

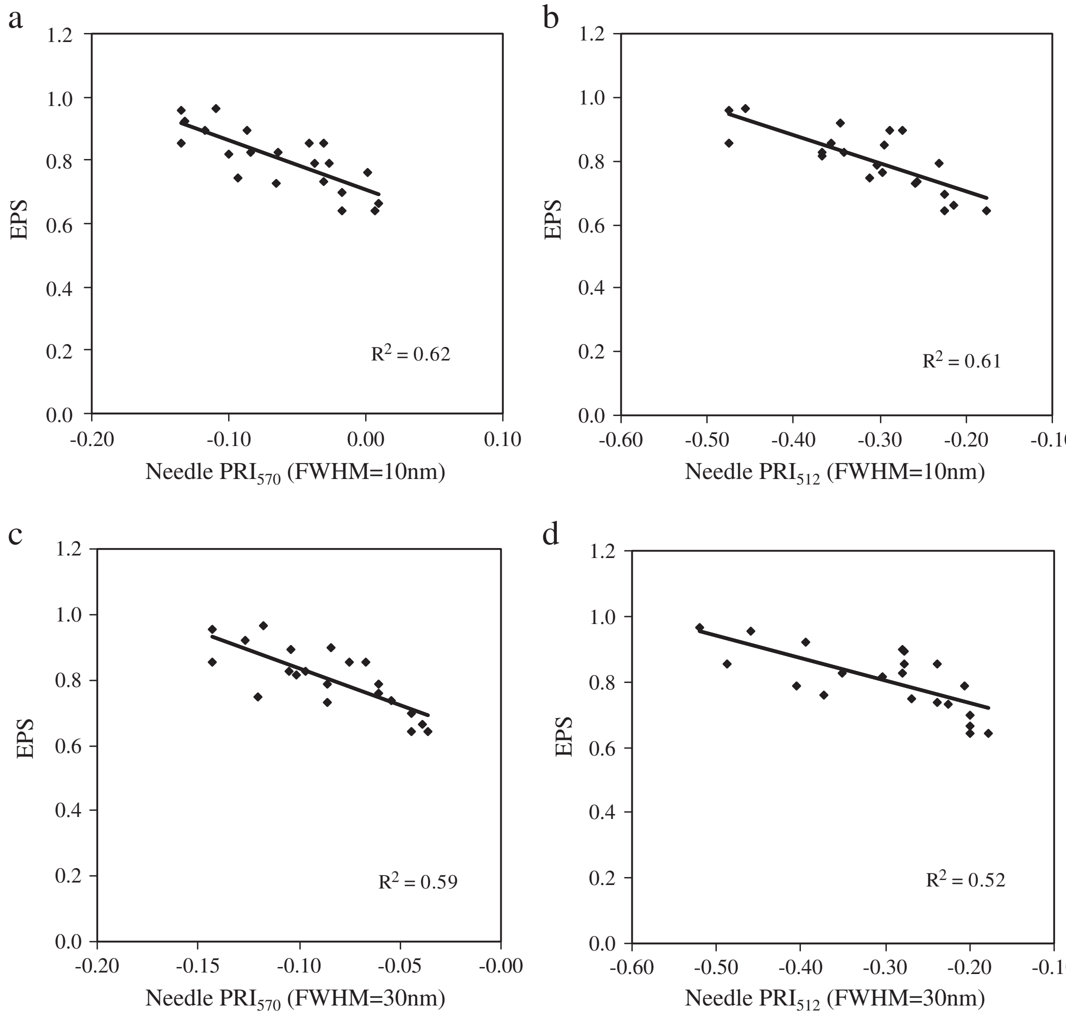

Fig. 12. Relationships obtained between the epoxidation state of the xanthophylls pigments EPS = (V + 0.5 A) / (V + A + Z) and PRI_{570} for FWHM of 10 nm (a) and 30 nm (c), and PRI_{512} with FWHM of 10 nm (b) and 30 nm (d). Needle measurements obtained at 12:00 GMT from crowns with different levels of stress on *Pinus nigra*.

Arbitrarily Inclined Leaves (SAILH) (Verhoef, 1984, 1985), coupled with LIBERTY for this study. Neither FLIM nor INFORM incorporates a correction to account for the fact that, in coniferous forests, needles are densely clumped into shoots. Such correction has been suggested by Nilson and Ross (1997) and Smolander and Stenberg (2003). However, INFORM is an innovative hybrid model with crown transparency, infinite crown reflectance and understory reflectance simulated using physically based sub-models. Hybrid models are combinations of geometrical and turbid medium models, therefore with INFORM tree crowns are not considered opaque but rather treated as a turbid medium. This factor plays an important role in conifer Mediterranean forests characterized by heterogeneous structures, thin leafy canopies and mutually shaded crowns.

A total of 125 simulations were performed with the LIBERTY + INFORM coupled model, varying LAI (1–3), tree density (800–2800 trees/ha), and chlorophyll concentration (100–500 mg/m^2). The simulated spectral reflectance dataset was used to calculate the vegetation indices under analysis: PRI_{570}, modified PRI formulations, and PRI indices normalized by the NDVI, SR, OSAVI, MSAVI and MTVI2 structural indices (Table 4). Model simulations were conducted for each PRI formulation to assess the effects of the reference band on PRI. The purpose of the simulation analysis was to assess the effects of the variability found in a pine forest on the simulated PRI formulations as a function of i) LAI; ii) fractional cover; and iii) Cab concentration. Model assessments and comparison against ground-measured EPS both at leaf and canopy levels were conducted.

3. Results

3.1. Model simulations

Model simulations conducted with LIBERTY for *P. nigra* needles using the PROSPECT chlorophyll absorption coefficient (k_{ab}) revealed good agreement when compared with needle spectra measured with the integrating sphere (Fig. 5). In contrast, LIBERTY simulations conducted with the original chlorophyll absorption coefficient (Dawson et al., 1998) reported a significant failure to match the needle reflectance measured in the 500–700 nm region (Fig. 5a and b). Input parameters and ranges used for the coupled LIBERTY + INFORM model (Table 5) were estimated by the inversion of 128 needle spectra measured in the laboratory with the integrating sphere for both species. At the canopy level, the coupled model was assessed against the reflectance extracted from the AHS data for study areas from both species. Fig. 5c shows good agreement between the reflectance spectra obtained from the AHS image and those simulated with the LIBERTY + INFORM coupled model for one of the study areas.

The LIBERTY + INFORM coupled model was used to assess the effects of canopy architecture on PRI and on the proposed PRI formulations (Table 4). A comparison between the coefficient of variation (CV) for each PRI reference band was conducted to assess the PRI formulation showing less variation as a function of LAI, tree density and chlorophyll content. Fig. 6 shows the mean, the CV, and the standard deviation of simulated spectral reflectance for a range of LAI and tree densities. The simulations were conducted for LAI values of 1 to 3, and tree densities in the range of 800–2800 trees/ha. The remaining inputs were set to the mean nominal values (Table 5). The CV obtained from each reference band (R_{512}, R_{570}, R_{600} and R_{670}) was 4.35%, 5.28%, 5.02% and 13.52%, respectively. Although the differences among the CV of the reference bands were no greater than 15%, R_{512} had the lowest value (Fig. 6). However, such differences increased when calculating the CV for PRI formulations, yielding CV = 48.98% for PRI_{570} and CV = 22.05% for PRI_{512}, demonstrating that PRI_{570} had a higher variation than other PRI formulations such as PRI_{512}. These theoretical results suggest that PRI_{512} is less sensitive to changes in LAI and tree densities than PRI_{570}. The effect of chlorophyll concentration was also studied by simulating a range of chlorophyll (100–500 mg/m^2), in addition to the variation in LAI (1–3) and tree density (800–2800 trees/ha). In this case, the CV for PRI_{570} decreased slightly (CV = 30.48%), while PRI_{512} remained almost invariant (CV = 23.01%). These results suggest that PRI_{512} is less sensitive to structural parameters and chlorophyll variations than PRI_{570}.

The structural effects on PRI formulations are shown as normalized for LAI = 1 (Fig. 7), showing the variation in PRI_{570} and PRI_m for a range of LAI and tree densities (Fig. 7 a, b, c and d). The variation in PRI_{m1} and PRI_{m4} was less significant than that of the rest of the PRI formulations (PRI_{570}, PRI_{m2}, and PRI_{m3}). Such differences were even greater when tree density or LAI increased. The patterns tracked by PRI_{570} *vs* PRI_{m1} as simulated for a range of LAI and tree density values (Fig. 8) demonstrate the lower sensitivity of PRI_{m1} to canopy structural changes than PRI_{570}. These results demonstrate the smaller effect caused by the tree density on PRI_{512} as compared to PRI_{570}.

Model simulations for canopy PRI_{570} and PRI_m indices were also conducted with LIBERTY + INFORM for assessing index variation as a function of chlorophyll concentration (Fig. 9). Simulations performed for increasing tree densities (Fig. 9a (800 trees/ha); Fig. 9b (1300 trees/ha); and Fig. 9c (1800 trees/ha)) as a function of LAI and Cab demonstrate that PRI_{570} and PRI_{m1} are affected by Cab.

3.2. Experimental results

3.2.1. PRI measurements at the needle level

The assessment to study the relationship between PRI_{570} and the epoxidation state of the xanthophylls pigments (EPS) was conducted on the diurnal dataset acquired at the leaf level. The comparison between EPS at 8:00 and 12:00 GMT for *P. sylvestris* (Fig. 10a) and *P. nigra* (Fig. 10b) for each study area demonstrates the differences found on EPS as a function of the stress level. There were significant differences in EPS between study areas for both species at 12:00 GMT. Values were not significantly different at 8:00 GMT for *P. sylvestris* and *P. nigra*. However, both species displayed a similar pattern, as diurnal differences in EPS increased on the areas with higher stress.

Based on midday measurements, EPS showed a consistent pattern of decline on needle PRI_{570} and needle PRI_{512} data at 10 and 30 nm bandwidths for both *P. sylvestris* (Fig. 11) and *P. nigra* sites (Fig. 12). Results demonstrated a similar sensitivity of both PRI_{570} and PRI_{512} to EPS, yielding coefficients of determination of $r^2 = 0.61$ for PRI_{570} (Fig. 11a) and $r^2 = 0.59$ for PRI_{512} (Fig. 11b) for *P. sylvestris*, and $r^2 = 0.62$ for PRI_{570} (Fig. 12a) and $r^2 = 0.61$ for PRI_{512} (Fig. 12b) for *P. nigra*. A higher concentration of the photosynthetic active pigment violaxanthin over the whole xanthophyll pool corresponds with higher values of EPS, and consequently smaller stress levels, thus showing lower PRI values. Similar results were found at the leaf level in *Abies alba* (Peguero-Pina et al., 2007) and *P. sylvestris* (Filella et al., 2009) needles, and in *Q. coccifera* (Peguero-Pina et al., 2008) and *Prunus persica* (Suárez et al., 2010) leaves.

The PRI formulations were then calculated for a FWHM of 30 nm, simulating the airborne AHS sensor bandwidth. Results showed significant relationships between EPS and indices PRI_{570} and PRI_{512} for *P. sylvestris* and *P. nigra* (Figs. 11 and 12). The coefficients of determination obtained for both species were similar, $r^2 = 0.59$ for PRI_{570} (Fig. 11c) and $r^2 = 0.40$ for PRI_{512} (Fig. 11d) for *P. sylvestris*, and $r^2 = 0.59$ for PRI_{570} (Fig. 12c) and $r^2 = 0.57$ for PRI_{512} (Fig. 12d) for *P. nigra*. The comparison of the relationships obtained with a FWHM of 10 and 30 nm (Figs. 11 and 12) shows that the instrument FWHM affects the relationships between PRI and EPS, as expected. Nevertheless, results obtained at 30 nm FWHM yielded significant relationships between EPS and both PRI_{570} and needle PRI_{512}. Consistent relationships were also obtained when aggregating the needle spectra at the plot level using the FWHM of the airborne AHS sensor (later used to acquire the imagery). Results of these relationships are shown in Fig. 13, yielding coefficients of determination of $r^2 = 0.89$ for EPS *vs* PRI_{570} (Fig. 13a) and $r^2 = 0.73$ for EPS *vs* PRI_{512} (Fig. 13b).

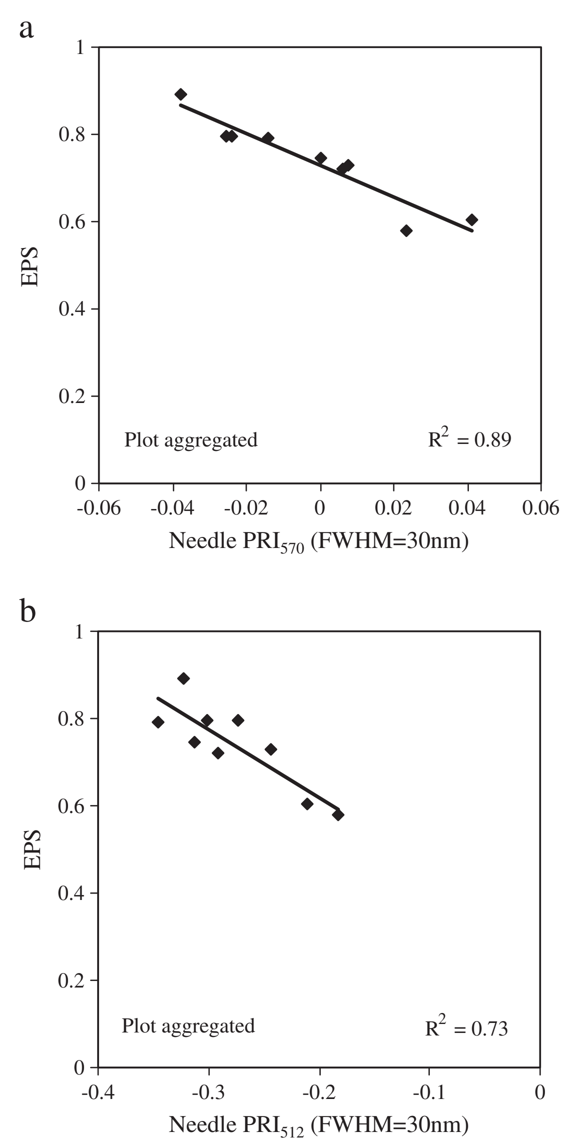

Fig. 13. Leaf-level relationships obtained between the epoxidation state of the xanthophylls pigments EPS = (V + 0.5 A)/(V + A + Z) and PRI_{570} (a) and PRI_{512} (b) both with FWHM of 30 nm. Needle measurements obtained at 12:00 GMT at the plot level with different levels of stress on *Pinus sylvestris*.

3.2.2. Results for PRI formulations at the canopy level

The study conducted to assess the relationships between field-measured EPS and crown-level PRI indices was conducted by selecting pixels with NDVI higher than 0.6 from windows of 3×3 pixels with center on the targeted crown. Vegetation indices assessed were PRI_{570}, and modified PRI formulations (PRI_{m1}, PRI_{m2}, PRI_{m3}, and PRI_{m4}), as well as the normalized modified PRI_{m1} indices over structural vegetation indices NDVI, SR, OSAVI, MSAVI and $MTVI_2$. Results showed that the airborne-level PRI indices were sensitive to EPS but, as expected were also highly affected by structural parameters. The relationships between EPS and indices PRI_{570}, PRI_{512}, NDVI and T are shown in Fig. 14. The index PRI_{512} shows higher relationships with EPS ($r^2=0.40$) than PRI_{570} ($r^2=0.21$) (Fig. 14a and b), demonstrating with the EPS *vs* NDVI relationship that structural effects due to stress were not the major driver (Fig. 14c) ($r^2=0.13$). Significant relationships were also found between T and EPS, although with lower coefficient of determination ($r^2=0.37$) (Fig. 14d). These results show that the relationship between PRI_{512} and EPS was stronger than with PRI_{570}. In agreement with the modeling results obtained, results show that PRI_{570} might be more affected by structural effects than PRI_{512}. According to the modeling results presented in Fig. 7, the PRI_{512} index seems less affected by structural effects than the PRI_{570} index for high tree densities (Fig. 7c and d) and slightly less or equally affected for low tree densities (Fig. 7a and b). Moreover, the normalized results (Fig. 8) show less LAI effects on PRI_{512} as compared to PRI_{570}. Besides the mentioned structural effects, clear differences can be seen between both indices under varying chlorophyll content (Fig. 9) where the pigment effects were smaller for PRI_{512}. In the field study, structural effects on the indices were further restricted by selecting pixels with NDVI>0.6, therefore targeting pure vegetation pixels and limiting the variation of the canopy structure. Under these conditions, the experimental results suggested a greater robustness of PRI_{512} for both canopy structure (tree density and LAI) and chlorophyll content variation.

Crown-level relationships also showed significant coefficients of determination between PRI_{512} and field-measured indicators of water stress such as Gs, ($r^2=0.45$) and Ψ, ($r^2=0.48$) (Fig. 15). In comparison, PRI_{570} yielded a coefficient of determination of $r^2=0.21$ (Gs) and $r^2=0.21$ (Ψ). These results demonstrate that PRI_{512} might be used as an indicator of water stress in conifer forest, and demonstrate the consistency with previously presented modeling results. Furthermore, these results are in agreement with the canopy results between EPS and PRI_{512}, which shows a superior performance for PRI_{512}. Other index modifications for PRI, such as PRI_{m2}, PRI_{m3} and PRI_{m4}, were shown to be very sensitive to structural parameters (data not included). The study conducted to assess the effects of normalizing PRI by structural vegetation indices such as

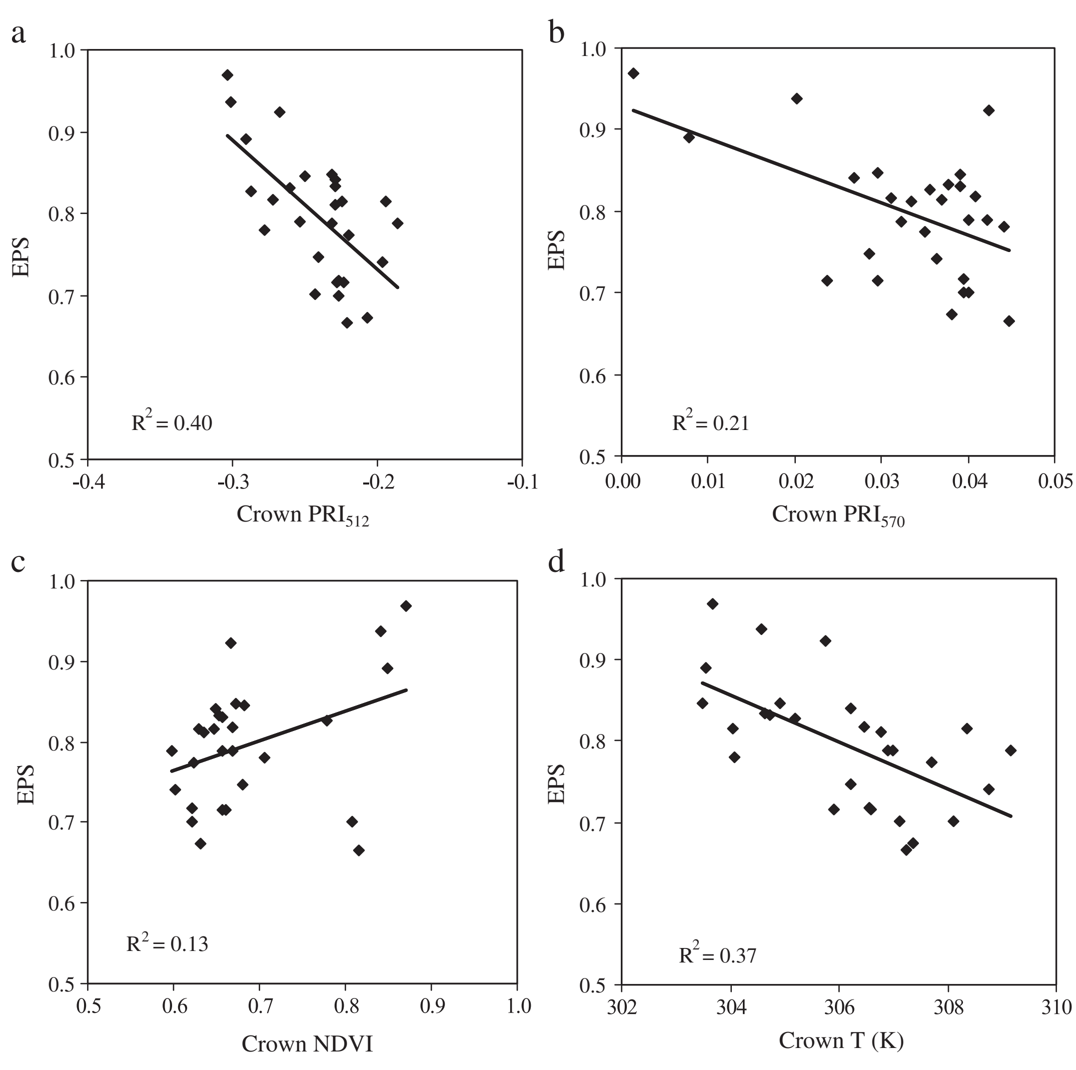

Fig. 14. Crown-level relationships obtained between the epoxidation state of the xanthophylls EPS (V + 0.5 A)/(V + A + Z) and vegetation indices: NDVI (a), PRI_{570} (b) and PRI_{512} (c). Needle measurements obtained at 12:00 GMT from crowns with different levels of stress on *Pinus sylvestris* and NDVI>0.6. PRI_{570}, PRI_{512} and T obtained from the AHS airborne sensor.

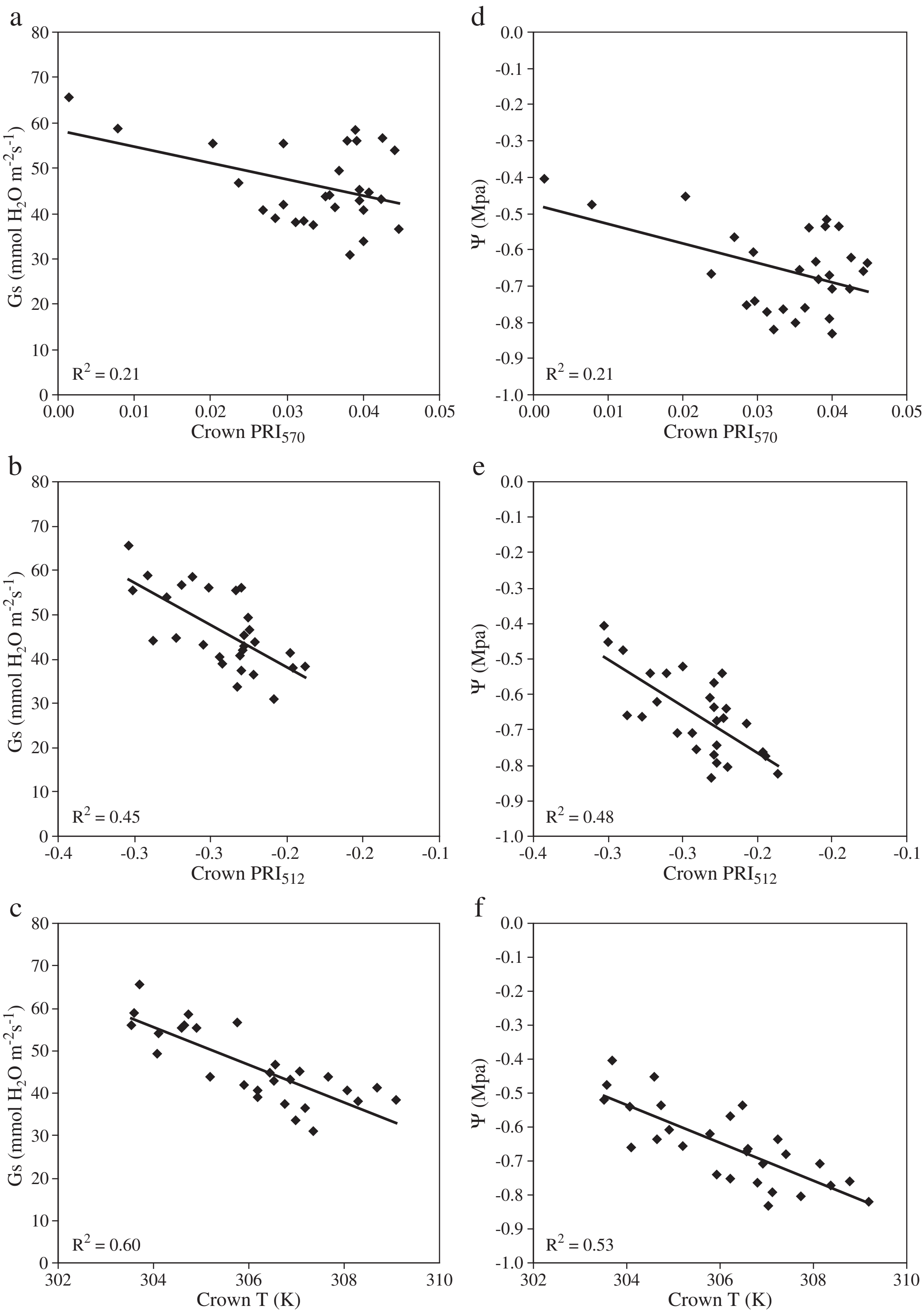

Fig. 15. Crown-level relationships obtained for *Pinus sylvestris* between the stomatal conductance (Gs) and PRI_{570} (a), PRI_{512} (b) and temperature (T) (c). Crown-level relationships between midday water potential (Ψ) and PRI_{570} (d), PRI_{512} (e) and temperature (T) (f) of trees with NDVI>0.6.

NDVI, SR, OSAVI and MSAVI indicated little improvement (data not included).

PRI_{570}, PRI_{m1} and NDVI were applied at the image level to map stress over the study areas. Fig. 16 shows the three *P. nigra* study areas (SN1, SN2, and SN3) and two zoomed images of each central plot at 1×1 and 3×3 resolution (pixel based) and at object level. A visual analysis reveals that the study areas with different stress levels showed similar NDVI and PRI_{570} values, but different PRI_{512} values (Fig. 16). To quantify these differences the mean and the standard deviation for each index were calculated for the four trees displayed in

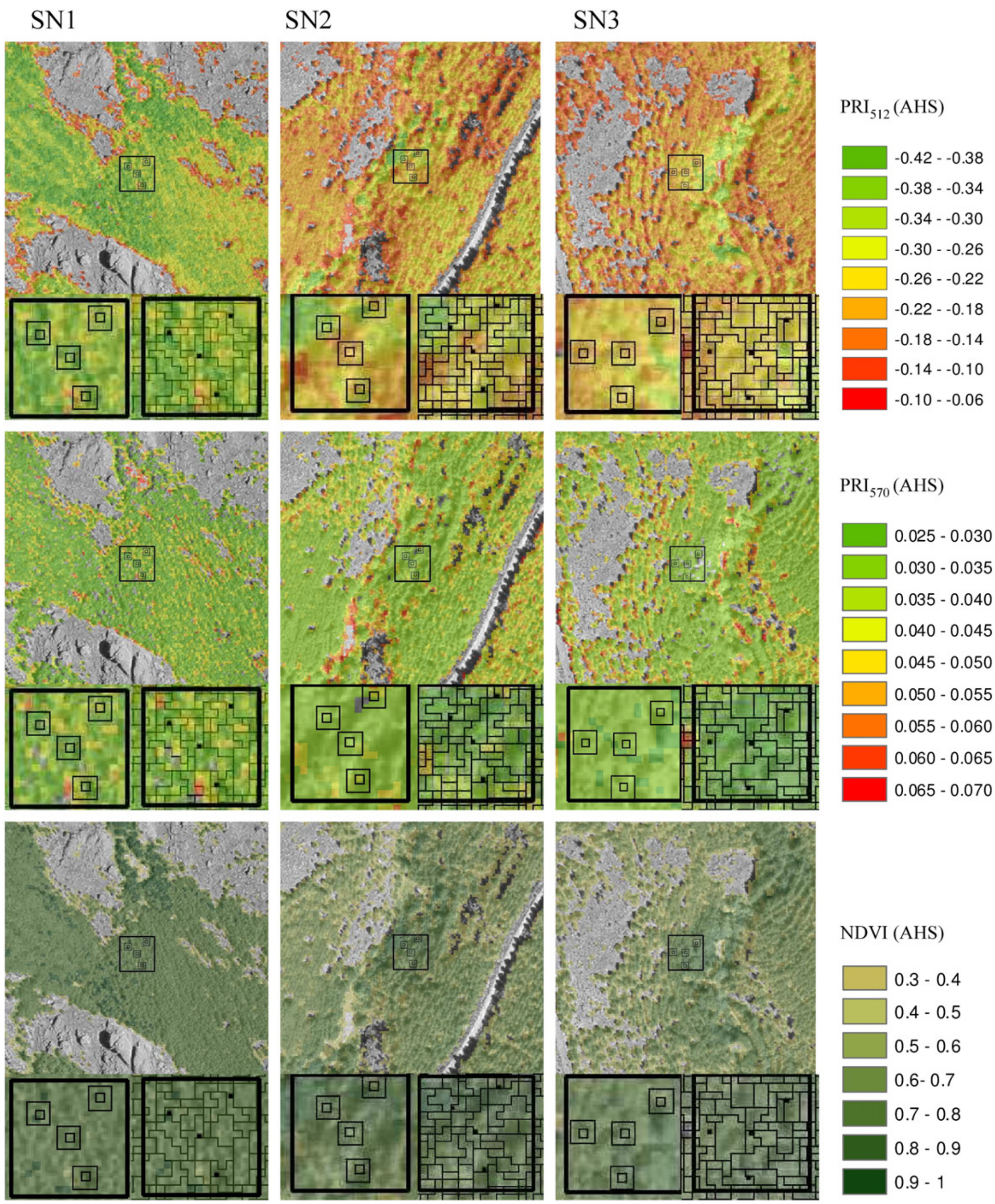

Fig. 16. PRI_{512}, PRI_{570} and NDVI obtained from the AHS airborne sensor from three study areas of *Pinus nigra* with different levels of stress: SN1, SN2 and SN3. At the bottom of each image, two zoom images of a central plot, one pixel-based displaying 1×1 and 3×3 resolutions and the other at object level.

the zoom images (Fig. 16), for a total of twelve trees for each species. While the mean values for NDVI and PRI_{570} were similar among the study areas, PRI_{512} showed different ranges for each stress level (Fig. 17a). A similar comparison was conducted for *P. sylvestris* (Fig. 17b). Simulation and experimental results were consistent with the mapping results obtained for PRI_{512}, showing its ability for accurately mapping stress at both pixel and object levels in conifer forests.

4. Conclusions

Radiative transfer simulation methods were applied using INFORM as a canopy reflectance model linked with a modified LIBERTY leaf model in order to assess the effects of canopy structure on different formulations of PRI. The simulations were conducted by computing canopy reflectance spectra with different values of LAI, tree density and chlorophyll content, assessing the effects of these biochemical and structural inputs on the proposed PRI formulations. The study demonstrated the sensitivity of PRI and modified PRI indices to canopy structural parameters and, therefore, the need for assessing robust PRI formulations with less structural effects. The simulation results demonstrate that PRI_{512} is less sensitive to changes in LAI values, tree densities and chlorophyll content than PRI_{570}.

In addition to the simulation work conducted, PRI indices were also tested using experimental data collected from the study sites at 8:00 and 12:00 GMT. Significant differences for both species were

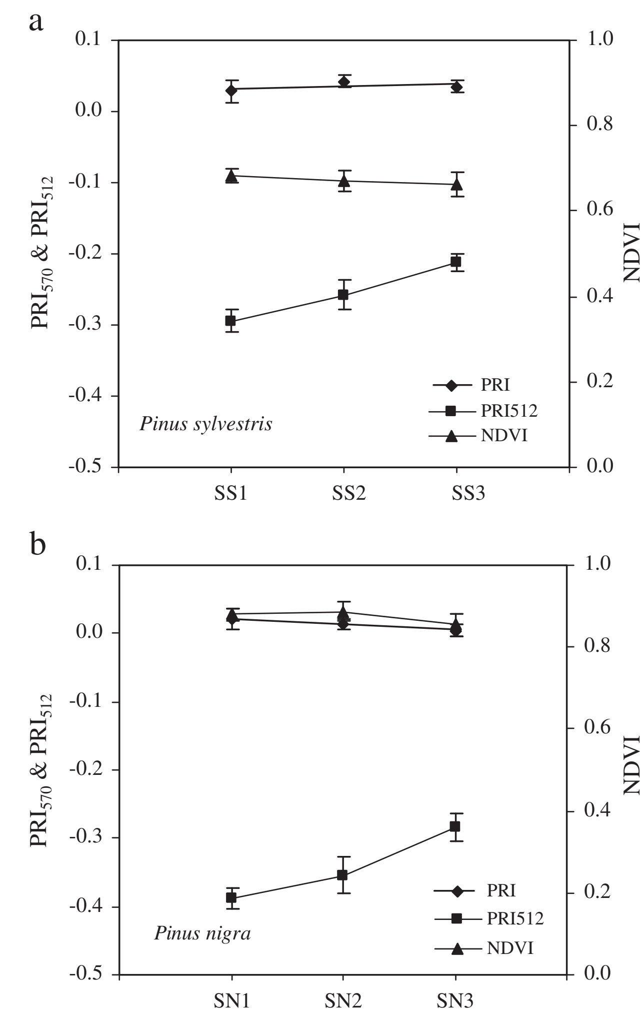

Fig. 17. Mean values and standard deviation obtained from the AHS image of PRI_{570}, PRI_{512} and NDVI. Values calculated from twelve trees located in the study areas SN1, SN2 and SN3 of *Pinus nigra* (a) and SS1, SS2 and SS3 of *Pinus sylvestris* (b).

found in EPS measured at 12:00 GMT as a function of the stress levels, showing that EPS declined consistently with PRI_{570} and PRI_{512}. At the leaf level, both PRI_{570} and PRI_{512} were sensitive to EPS measured by destructive sampling. Nevertheless, the study conducted at the canopy level revealed that PRI_{512} was better correlated with EPS and physiological indicators, such as water potential and stomatal conductance, than PRI_{570}. The better performance obtained for PRI_{512} over PRI_{570} at the canopy level in the experimental study confirms the modeling results which showed the lower sensitivity of PRI_{512} to structural effects in conifer canopies as compared to PRI_{570}. Other formulations such as PRI_{m2}, PRI_{m3} and PRI_{m4} were highly sensitive to structural parameters and therefore not optimum for stress detection in these canopies. The sensitivity of the PRI indices to structural parameters is critical in conifer forests, where the heterogeneity allows greater influence due to the ground layer and shadows.

This work demonstrates the link between PRI_{512} and PRI_{570} with EPS in *P. sylvestris* and *P. nigra* at the leaf level, and it suggests the superior performance at the canopy level for PRI_{512}*vs* PRI_{570} when mapping pre-visual stress levels in conifer forests.

Acknowledgements

Financial support from EGMASA (Environmental Management Company, Ltd.) and the Environmental Ministry of the Regional Andalusian Government, and partial support from the Innovation and Development Agency of Andalusia (Regional Ministry of Innovation, Science and Enterprise), are gratefully acknowledged, as well as support from the GESBOME project (Regional Andalusian GovernmentP06-RNN-1890) and Aragón Government (A03 research group). J. E. Frieyro de Lara, A. Hayas-López, Rafael Sánchez and David Ariza are acknowledged for measurements and technical support in the field campaigns, and A. Calviño for technical help with the HPLC measurements. J. E. Granados and the members of CAHA (German–Spanish Astronomical Center at Calar Alto), Eustaquio Gil-Pelegrín and J. J. Peguero-Pina (CITA, Zaragoza) are acknowledged for technical support.

References

Abadía, A., & Abadía, J. (1993). Iron and plant pigments. In L. L. Barton, & B. C. Hemming (Eds.), *Iron chelation in plants and soil microorganisms* (pp. 327–344). San Diego: Academic.

Allen, C. D., Macalady, A. K., Chenchouni, H., Bachelet, D., McDowell, N., Vennetier, M., et al. (2009). A global overview of drought and heat-induced tree mortality reveals emerging climate change risks for forests. *Forest Ecology and Management*, *259*, 660–684.

Asner, G. P., Carlson, K. M., & Martin, R. E. (2005). Substrate age and precipitation effects on Hawaiian forest canopies from spaceborne imaging spectroscopy. *Remote Sensing of Environment*, *98*, 457–467.

Atzberger, C. (2000). Development of an invertible forest reflectance model: The INFOR-model. In Buchroithner (Ed.), *A Decade of Trans-European Remote Sensing Cooperation. Proceedings of the 20th EARSeL Symposium, Dresden, Germany, 14–16 June 2000*. (pp. 39–44).

Barton, C. V. M., & North, P. R. J. (2001). Remote sensing of canopy light use efficiency using the Photochemical Reflectance Index. Model and analysis. *Remote Sensing of Environment*, *78*, 264–273.

Berk, A., Anderson, G. P., Acharya, P. K., Chetwynd, J. H., Bernstein, L. S., Shettle, E. P., et al. (2000). *MODTRAN4 user's manual.* Hanscom MA: Air Force Research Laboratory.

Berk, A., Bernstein, L. S., Anderson, G. P., Acharya, P. K., Robertson, D. C., Chetwynd, J. H., et al. (1998). MODTRAN cloud and multiple scattering upgrades with application to AVIRIS. *Remote Sensing of Environment*, *65*, 367–375.

Berni, J. A. J., Zarco-Tejada, P. J., Sepulcre-Cantó, G., Fereres, E., & Villalobos, F. J. (2009). Mapping stomatal conductance and CWSI in olive orchards using high resolution thermal remote sensing imagery. *Remote Sensing of Environment*, *113*, 2380–2388.

Björkman, O., & Demmig-Adams, B. (1994). Regulation of photosynthetic light energy capture, conversion, and dissipation in leaves of higher plants. In D. E. Schulze, & M. M. Caldwell (Eds.), *Ecophysiology of photosynthesis* (pp. 17–45). Berlin, Germany: Springer-Verlag.

Dawson, T. P., Curran, P. J., & Plummer, S. E. (1998). LIBERTY — Modelling the effects of leaf biochemical concentration on reflectance spectra. *Remote Sensing of Environment*, *65*, 50–60.

Demmig-Adams, B., & Adams, W. W. (1996). The role of xanthophyll cycle carotenoids in the protection of photosynthesis. *Trends in Plant Science*, *1*, 21–26.

Di Vittorio, A. V. (2009). Enhancing a leaf radiative transfer model to estimate concentrations and *in vivo* specific absorption coefficients of total carotenoids and chlorophylls *a* and *b* from single-needle reflectance and transmittance. *Remote Sensing of Environment*, *113*, 1948–1966.

Drolet, G. G., Huemmrich, K. F., Hall, F. G., Middleton, E. M., Black, T. A., Barr, A. G., et al. (2005). A MODIS-derived Photochemical Reflectance Index to detect inter-annual variations in the photosynthetic light-use efficiency of a boreal deciduous forest. *Remote Sensing of Environment*, *98*, 212–224.

Filella, I., Amaro, T., Araus, J. L., & Peñuelas, J. (1996). Relationship between photosynthetic radiation-use efficiency of barley canopies and the photochemical reflectance index (PRI). *Physiologia Plantarum*, *96*, 211–216.

Filella, I., Porcar-Castell, A., Munné-Bosch, S., Bäck, J. M., Garbulsky, F., & Peñuelas, J. (2009). PRI assessment of long-term changes in carotenoids/chlorophyll ratio and short-term changes in de-epoxidation state of the xanthophyll cycle. *Remote Sensing of Environment*, *30*, 4443–4455.

Gamon, J. A., Filella, I., & Peñuelas, J. (1993). The dynamic 531 nm reflectance signal: A survey of twenty angiosperm species. In H. Y. Yamamoto, & C. M. Smith (Eds.), *1993, Photosynthetic responses to the environment* (pp. 172–177). Rockville, MD: American Society of Plant Physiologists.

Gamon, J. A., Peñuelas, J., & Field, C. B. (1992). A narrow-waveband spectral index that tracks diurnal changes in photosynthetic efficiency. *Remote Sensing of Environment*, *41*, 35–44.

Gamon, J. A., Serrano, L., & Surfus, J. S. (1997). The photochemical reflectance index: An optical indicator of photosynthetic radiation use efficiency across species, functional types and nutrient levels. *Oecologia*, *112*, 492–501.

Garbulsky, M. F., Peñuelas, J., Papale, D., & Filella, I. (2008). Remote estimation of carbon dioxide uptake by a Mediterranean forest. *Global Change Biology*, *14*, 2860–2867.

Haboudane, D., Miller, J. R., Pattey, E., Zarco-Tejada, P. J., & Strachan, I. B. (2004). Hyperspectral vegetation indices and novel algorithms for predicting green LAI of crop canopies: Modeling and validation in the context of precision agriculture. *Remote Sensing of Environment*, *90*, 337–352.

Hall, F. G., Hilker, T., Coops, N. C., Lyapustin, A., Huemmrich, K. F., Middleton, E. M., et al. (2008). Multi-angle remote sensing of forest light use efficiency by observing PRI

variation with canopy shadow fraction. *Remote Sensing of Environment*, *112*, 3201–3211.
Hilker, T., Coops, N. C., Hall, F. G., Black, T. A., Wulder, M. A., Nesic, Z., et al. (2008). Separating physiologically and directionally induced changes in PRI using BRDF models. *Remote Sensing of Environment*, *112*, 2777–2788.
Hilker, T., Lyapustin, A., Hall, F. G., Wang, Y., Coops, N. C., Drolet, G., et al. (2009). An assessment of photosynthetic light use efficiency from space: Modeling the atmospheric and directional impacts on PRI reflectance. *Remote Sensing of Environment*, *113*, 2463–2475.
Inoue, Y., Peñuelas, J., Miyata, A., & Mano, M. (2008). Normalized difference spectral indices for estimating photosynthetic efficiency and capacity at a canopy scale derived from hyperspectral and CO_2 flux measurements in rice. *Remote Sensing of Environment*, *112*, 156–172.
Jackson, R. D., Reginato, R. J., & Idso, S. B. (1977). Wheat canopy temperature: A practical tool for evaluating water requirements. *Water Resources Research*, *13*, 651–656.
Jordan, C. F. (1969). Derivation of leaf area index from quality of light on the forest floor. *Ecology*, *50*, 663–666.
Larbi, A., Abadía, A., Morales, F., & Abadía, J. (2004). Fe resupply to Fe-deficient sugar beet plants leads to rapid changes in the violaxanthin cycle and other photosynthetic characteristics without significant *de novo* chlorophyll synthesis. *Photosynthesis Research*, *79*, 59–69.
Malenovsky, Z., Albrechtova, J., Lhotakova, Z., Zurita-Milla, R., Clevers, G. P. W., Schaepman, M. E., et al. (2006). Applicability of the PROSPECT model for Norway spruce needles. *International Journal of Remote Sensing*, *27*, 5315–5340.
Martínez-Vilalta, J., López, B. C., Adell, N., Badiella, L., & Ninyerola, M. (2008). Twentieth century increase of Scots pine radial growth in NE Spain shows strong climate interactions. *Global Change Biology*, *14*, 2868–2881.
Melamed, N. T. (1963). Optical properties of powders. Part I. Optical absorption coefficients and the absolute value of the diffuse reflectance. Part II. Properties of luminescent powders. *Applied Optics*, *34*, 560–570.
Melzack, R. N., Bravdo, B., & Riov, J. (1985). The effect of water stress on photosynthesis and related parameters in *Pinus halepensis*. *Physiologia Plantarum*, *64*, 295–300.
Middleton, E. M., Cheng, Y. B., Hilker, T., Black, T. A., Krishnan, P., Coops, N. C., et al. (2009). Linking foliage spectral responses to canopy level ecosystem photosynthetic light use efficiency at a Douglas-fir forest in Canada. *Canadian Journal of Remote Sensing*, *35*, 166–188.
Moorthy, I., Miller, J. R., & Noland, T. L. (2008). Estimating chlorophyll concentration in conifer needles with hyperspectral data: An assessment at the needle and canopy level. *Remote Sensing of Environment*, *112*, 2824–2838.
Navarro-Cerrillo, R. M., Varo, M. A., Lanjeri, S., & Hernández-Clemente, R. (2007). Cartografía de defoliación en los pinares de pino silvestre (*Pinus sylvestris* L.) y pino salgareño (*Pinus nigra* Arnold) en la Sierra de los Filabres. *Ecosistemas*, *16*, 163–171.
Nilson, T., & Ross, J. (1997). Modeling radiative transfer through forest canopies: Implications for canopy photosynthesis and remote sensing. In H. L. Gholz, K. Nakane, & H. Shimoda (Eds.), *The use of remote sensing in the modeling of forest productivity* (pp. 23–60). Dordrecht: Kluwer.
Peguero-Pina, J. J., Camarero, J. J., Abadía, A., Martín, E., González-Cascón, R., Morales, F., et al. (2007). Physiological performance of silver-fir (*Abies alba* Mill.) populations under contrasting climates near the south-western distribution limit of the species. *Flora*, *202*, 226–236.
Peguero-Pina, J. J., Morales, F., Flexas, J., Gil-Pelegrín, E., & Moya, I. (2008). Photochemistry, remotely sensed physiological reflectance index and de-epoxidation state of the xanthophyll cycle in *Quercus coccifera* under intense drought. *Oecologia*, *156*, 1–11.
Peñuelas, J., Filella, I., & Gamon, J. A. (1995). Assessment of photosynthetic radiation use eficiency with spectral reflectance. *The New Phytologist*, *131*, 291–296.
Peñuelas, J., Gamon, J. A., Fredeen, A. L., Merino, J., & Field, C. B. (1994). Reflectance indices associated with physiological changes in nitrogen- and water-limited sunflower leaves. *Remote Sensing of Environment*, *48*, 135–146.
Poyatos, R., Llorens, P., Piñol, J., & Rubio, C. (2008). Response of Scots pine (*Pinus sylvestris* L.) and pubescent oak (*Quercus pubescens* Willd.) to soil and atmospheric water deficits under Mediterranean mountain climate. *Annals of Forest Science*, *65*, 306.
Qi, J., Chehbouni, A., Huete, A. R., & Kerr, Y. H. (1994). Modified Soil Adjusted Vegetation Index (MSAVI). *Remote Sensing of Environment*, *48*, 119–126.
Rebetez, M., & Dobbertin, M. (2004). Climate change may already threaten Scots pine stands in the Swiss Alps. *Theoretical and Applied Climatology*, *79*, 1–9.
Richardson, A. D., & Berlyn, P. (2002). Changes in foliar spectral reflectance and chlorophyll fluorescence of four temperate species following branch cutting. *Tree Physiology*, *22*, 499–506.
Rondeaux, G., Steven, M., & Baret, F. (1996). Optimization of soil-adjusted vegetation indices. *Remote Sensing of Environment*, *55*, 95–107.
Rosema, A., Verhoef, W., Noorbergen, H., & Borgesius, J. J. (1992). A new forest light interaction model in support of forest monitoring. *Remote Sensing of Environment*, *42*, 23–41.
Rouse, J. W., Haas, R. H., Schell, J. A., Deering, D. W., & Harlan, J. C. (1974). Monitoring the vernal advancement and retrogradation (Greenwave Effect) of natural vegetation. *Type III Final Report, NASA Goddard Space Flight Center, Greenbelt, Maryland, 20771, USA* 371 pp.
Schlerf, M., & Atzberger, C. G. (2006). Inversion of a forest reflectance model to estimate structural canopy variables from hyperspectral remote sensing. *Remote Sensing of Environment*, *100*, 281–294.
Schlerf, M., Atzberger, C. G., & Hill, J. (2005). Remote sensing of forest biophysical variables using HyMap imaging spectrometer data. *Remote Sensing of Environment*, *95*, 177–194.
Scholander, P. F., Hammel, H. T., Bradstreet, E. D., & Hemmingsen, E. A. (1965). Sap pressure in vascular plants. *Science*, *148*, 339–346.
Sepulcre-Cantó, G., Zarco-Tejada, P. J., Jiménez-Muñoz, J. C., Sobrino, J. A., de Miguel, E., & Villalobos, F. J. (2006). Detection of water stress in an olive orchard with thermal remote sensing imagery. *Agricultural and Forest Meteorology*, *136*, 31–44.
Sepulcre-Cantó, G., Zarco-Tejada, P. J., Jiménez-Muñoz, J. C., Sobrino, J. A., Soriano, M. A., Fereres, E., et al. (2007). Monitoring yield and fruit quality parameters in open-canopy tree crops under water stress. Implications for ASTER. *Remote Sensing of Environment*, *107*, 455–470.
Sepulcre-Cantó, G., Zarco-Tejada, P. J., Sobrino, J. A., Berni, J. A. J., Jiménez Muñoz, J. C., & Gastellu-Etchegorry, J. P. (2009). Detecting water status in open canopies with thermal ASTER imagery and DART radiative transfer simulation. *Agricultural and Forest Meteorology*, *149*, 962–975.
Sims, D. A., & Gamon, J. A. (2002). Relationships between leaf pigment content and spectral reflectance across a wide range of species, leaf structures and developmental stages. *Remote Sensing of Environment*, *81*, 337–354.
Smolander, S., & Stenberg, P. (2003). A method to account for shoot scale clumping in coniferous canopy reflectance models. *Remote Sensing of Environment*, *88*, 363–373.
Sobrino, J. A., Jiménez-Muñoz, J. C., Labed-Nachbrand, J., & Nerry, F. (2002). Surface emissivity retrieval from Digital Airborne Imaging Spectrometer data. *Journal of Geophysical Research*, *107*(D23), 4729. doi:10.1029/2002JD002197.
Sobrino, J. A., Jiménez-Muñoz, J. C., Zarco-Tejada, P. J., Sepulcre-Cantó, G., & de Miguel, E. (2006). Land surface temperature derived from airborne hyperspectral scanner thermal infrared data. *Remote Sensing of Environment*, *102*, 99–115.
Suárez, L., Zarco-Tejada, P. J., Berni, J. A. J., González-Dugo, V., & Fereres, E. (2009). Modelling PRI for water stress detection using radiative transfer models. *Remote Sensing of Environment*, *113*, 730–744.
Suárez, L., Zarco-Tejada, P. J., González-Dugo, V., Berni, J. A. J., Sagardoy, R., Morales, F., et al. (2010). Detecting water stress effects on fruit quality in orchards with time-series PRI airborne imagery. *Remote Sensing of Environment*, *114*, 286–298.
Suárez, L., Zarco-Tejada, P. J., Sepulcre-Cantó, G., Pérez-Priego, O., Miller, J. R., Jiménez-Muñoz, J. C., et al. (2008). Assessing canopy PRI for water stress detection with diurnal airborne imagery. *Remote Sensing of Environment*, *112*, 560–575.
Thayer, S. S., & Björkman, O. (1990). Leaf xanthophyll content and composition in sun and shade determined by HPLC. *Photosynthesis Research*, *23*, 331–343.
Verhoef, W. (1984). Light scattering by leaf layers with application to canopy reflectance modeling: The SAIL model. *Remote Sensing of Environment*, *16*, 125–141.
Verhoef, W. (1985). Earth observation modeling based on layer scattering matrices. *Remote Sensing of Environment*, *17*, 165–178.
Yamamoto, Y. (1979). Biochemistry of the violaxanthin cycle in higher plants. *Pure & Applied Chemistry*, *51*, 639–648.
Zarco-Tejada, P. J., Miller, J. R., Harron, J., Hu, B., Noland, T. L., Goel, N., et al. (2004). Needle chlorophyll content estimation through model inversion using hyperspectral data from boreal conifer forest canopies. *Remote Sensing of Environment*, *89*, 189–199.
Zhang, Y., Chen, J. M., Miller, J. R., & Noland, T. L. (2008). Retrieving chlorophyll content of conifer needles from hyperspectral measurements. *Canadian Journal of Remote Sensing*, *34*, 296–310.